# Resonant instability mode triads in the compressible boundary layer flow over a swept wing

M. P. Vonderwell and D. N. Riahi
Department of Theoretical and Applied Mechanics
216 Talbot Laboratory, 104 S. Wright Street
University of Illinois
Urbana, Illinois 61801 USA

## ABSTRACT

Instability modes that satisfy the triad resonance conditions in three-dimensional compressible (subsonic) boundary layer flow over a swept wing are investigated using theoretical and computational methods. Detuning parameters are used for the wave numbers and frequencies for the triad resonance conditions in space and time. Different resonant triads comprised of crossflow and Tollmien-Schlichting modes are investigated for both the incompressible and compressible cases. The effects of compressibility on various flow features, instability modes, and wave interactions are determined.

## I. INTRODUCTION

This paper studies the evolution of resonant instability mode triads in the compressible (subsonic) three-dimensional boundary layer flow over a swept wing. The resonant instability mode triad is an important wave interaction process which can take place early in the evolution of linear instability modes, and can subsequently affect the nonlinear evolution and transition from laminar to turbulent flow. An understanding of the triads processes can be useful, in particular, for design of aircraft wings and the related optimization of laminar flow control methods leading to drag reduction.

Three-dimensional boundary layers are subject to crossflow instability as well as the Tollmien-Schlichting (TS) modes observed in two-dimensional layers. Crossflow modes

(CF) dominate at the leading edge of the wing, while TS modes show larger growth rates in the mid-chord region. In between, there is a region where both CF and TS modes are present. What effect the two types of modes might have on one another is not known. Laminar flow control methods, such as distributed weak suction on the wing's surface, are often designed based upon the linear stability theory and the $e^N$ transition criterion. A nonlinear interaction among these modes might thwart the laminar flow control effort by causing unexpected transition to turbulence.

In aerodynamic applications, the three-dimensional boundary layer flows are compressible in nature. The effects of compressibility on the resonant triads is therefore an important consideration that is addressed in the present paper.

Resonant wave triads have been investigated by a number of authors in the past. Craik [1,2] established the existence of resonant instability mode triads in flow over a flat plate and discovered a significant wave interaction. Lekoudis [3] confirms the existence of a resonant triad on a swept wing which consisted of three traveling crossflow modes, but the interaction coefficients and amplitudes of these modes were not calculated. El-Hady [4] presented computational results for some resonant instability mode triads in a three dimensional boundary layer flow using an incompressible theory. Detuning parameters were used and nonparallel effects were taken into account. He concluded, in particular, that for a triad consisting of two traveling and one stationary crossflow mode, strong amplification of the traveling crossflow modes can occur. For a triad consisting of two Tollmien-Schlichting (TS) and one stationary crossflow mode, strong amplification of the TS modes is possible according to his calculations, provided the initial TS amplitudes are sufficiently small.

In some sense, the present work can be considered an extension of the work of El-Hady [4] to include the compressibility effects in the subsonic regime. For the compressible case, the expressions for a number of quantities, such as the interaction coefficients, become quite lengthy so these expressions, which have been double checked

by the authors using computer tool (mathematica) and by hand, will not be presented in this paper. The reader will instead be referred to Vonderwell [5] for complete presentations of these expressions and for greater details of various aspects of the present subject. Also the analysis and the formulation of the problem is described in details by El-Hady [4] in the incompressible limit and Vonderwell [5] in the compressible case. Thus, the analysis and the formulation will be presented briefly in the present paper.

## II. FORMULATION

The compressible Navier-Stokes, continuity, state, and energy equations [6] are the basic equations of the present wave interaction investigation. To apply them to the flow over a swept wing, we first select a local cartesian coordinate system with the x-z plane tangent to the wing surface and the y-axis perpendicular in the transverse direction. The x-axis is directed along the chord and the z-axis along the span. The complete basic Navier-Stokes, continuity, state, and energy equations are given by Schlichting [6] and will not be repeated here. We nondimensionalize these equations making use of the boundary layer displacement thickness, $\delta^*$, as the reference length, the free stream velocity magnitude, $U_\infty^*$, as the reference velocity, and the corresponding free stream quantities, $\Theta_\infty^*$, $\rho_\infty^*$, $\mu_\infty^*$, $k_\infty^*$, $\rho_\infty^* U_\infty^{*2}$, as reference temperature, density, viscosity, thermal conductivity, and pressure, respectively. This yields the nondimensional set of the governing equations for the total (base flow plus disturbance) quantities [5]. In these equations u, v, and w are the components of velocity in the x, y, and z directions, respectively, $\Theta$ is the temperature, P is the pressure, $\mu$ is the dynamic viscosity, $k$ is the thermal conductivity, $M = U_\infty^* / c_\infty^*$ is the boundary layer edge Mach number, $c_\infty^*$ is the free stream speed of sound, $R = \rho_\infty^* U_\infty^* \delta^* / \mu_\infty^*$ is the Reynolds number, $\mathrm{Pr} = \mu_\infty^* c_v^* / k_\infty^*$ is the Prandtl number, and $\gamma = c_p^* / c_v^*$ is the ratio of specific heats at constant pressure and volume. In the following formulation, the subscripts t, e, w and 0 indicate a total value, the value at the boundary layer edge, the value of a quantity at the wing surface, and the base flow quantity, respectively. The boundary conditions considered are those for an

adiabatic wing with weak suction [4]. We assume the coefficient of bulk viscosity is zero [6], the coefficients of viscosity and thermal conductivity are functions of temperature, and the Sutherland law [7] is used to determine $\mu$ and $k$.

The steady state base flow solution considered here satisfies the laminar boundary layer system [6] for a 23° swept infinite span wing.

We consider the stability of such base flow over the swept wing with particular interest in the weakly nonlinear interaction of resonant triads of linear instability modes. The stability analysis begins with a perturbation of the base flow yielding a system for the perturbation quantities. We anticipate, at leading order, a linear system for the perturbation quantities which yields periodic solutions with amplitudes that can grow or decay slowly in time or space. At higher order, we expect some weak modulation of the amplitude due to the effects of the weakly nonlinear triad and some modulation due to weakly nonparallel growth of order $\varepsilon_1(\varepsilon_1 << 1)$ of the boundary layer. Making use of the method of multiple scales to determine the wave packet solution of the governing system [4], we introduce the slowly varying variables

$$x_s = \varepsilon x, \qquad z_s = \varepsilon z, \qquad t_s = \varepsilon t, \tag{1}$$

where small parameter, $\varepsilon$, characterizes the magnitude of the disturbance quantity. We now pose as a solution to the basic governing systems expansions in powers of $\varepsilon$ of the form

$$u_t = u_0(x_s, y, z_s) + \varepsilon u_1(x, y, z, t, x_s, z_s, t_s) + \varepsilon^2 u_2(x, y, z, t, x_s, z_s, t_s) + \ldots \tag{2}$$

with a similar expansions for the other dependent variables for the total quantities. For the total viscosity we assume an expansion of the form

$$\mu_t = \mu_0(\theta_0) + \varepsilon \frac{d\mu}{d\theta}\theta_1 + \ldots \tag{3}$$

with a similar expansion for the total thermal conductivity $k_t$. Substitution of these

expansions into the system for the total quantities, subtraction of the base flow system, and collection of coefficients of equal powers of $\varepsilon$ leads to systems of equations at each order of $\varepsilon$. At order $\varepsilon$, the linear stability system can be written in the following form

$$L_i(u_1, v_1, w_1, \theta_1, p_1, \rho_1) = 0, \quad (i = 1,...,6), \tag{4a}$$

$$u_1 = v_1 = w_1 = \theta_1 = 0 \ \text{ at } \ y = 0, \infty, \tag{4b}$$

where $L_i$ are linear operators whose expressions are lengthy [5] and will not be given here. We seek a solution to (4) in the form of a superposition of three modes as follows:

$$(u_1, v_1, w_1, \theta_1, p_1, \rho_1) = \sum_{n=1}^{3} a_n(x_s, z_s, t_s) e^{i\phi_n} (u_{1n}, v_{1n}, w_{1n}, \theta_{1n}, p_{1n}, \rho_{1n}) + c.c. \tag{5a}$$

where $c.c.$ denotes the complex conjugate, $a_n$ is the disturbance amplitude, and

$$\left(\frac{\partial}{\partial x}, \frac{\partial}{\partial z}, \frac{\partial}{\partial t}\right)\phi_n = \left[\alpha_n(x_s, z_s), \beta_n(x_s, z_s), \omega_n(x_s, z_s)\right]. \tag{5b}$$

Here, $\alpha_n$, $\beta_n$, and $\omega_n$ are the wave number in the x-direction, the wave number in the z-direction, and the frequency of the disturbance. The wave numbers and frequencies are all, in general, complex. To form a triad, we require that

$$(\alpha_{3r}, \beta_{3r}, \omega_{3r}) = (\alpha_{1r}, \beta_{1r}, \omega_{1r}) + (\alpha_{2r}, \beta_{2r}, \omega_{2r}) + \varepsilon(\sigma_\alpha, \sigma_\beta, \sigma_\omega), \tag{6}$$

where the subscript $r$ indicates the real part and the so called detuning parameters contained in the last term on the right side of (6) represents the deviation from perfect resonance. The detuning parameters are introduced in (6) to express quantitatively the nearness of the resonances. It turns out that near resonance cases occur more often than perfect resonance where the detuning parameters are all zero. Using (5) in (4) yields the following system [5].

$$L_i(u_{1n}, v_{1n}, w_{1n}, \theta_{1n}, p_{1n}, \rho_{1n}) = 0, \quad (i = 8,...,13), \tag{7a}$$

$$u_{1n} = v_{1n} = w_{1n} = \theta_{1n} = 0 \ \text{ at } \ y = 0, \infty, \tag{7b}$$

where $L_i$ are linear operators applied on the subscript '$1n$' quantities whose expressions are lengthy [5] and will not be given here.

The above system is homogeneous and therefore has a nontrivial solution only for certain combinations of values of $\alpha_n$, $\beta_n$, and $\omega_n$. To order $\varepsilon^2$, the stability system can be written in the form

$$L_i(u_2, v_2, w_2, \theta_2, p_2, \rho_2) = N_i, \quad (i = 1,...,6), \tag{8a}$$

$$u_2 = v_2 = w_2 = \theta_2 = 0 \ \text{ at } \ y = 0, \infty, \tag{8b}$$

where the nonlinear and non- parallel terms, $N_i$, are very lengthy [5] and will not be given here. The non-parallel terms, which are of order $\varepsilon_1\varepsilon$ in the present formulation, are included in the expressions $N_i$ so that when the results over distances of order one disturbance wavelength or less is considered or when $\varepsilon_1 << \varepsilon$, then the non-parallel terms can be discarded, and when $\varepsilon_1 = 0(\varepsilon)$, they can be retained in the order $\varepsilon^2$ system [4]. The only two other ways known presently to incorporate the combined nonlinear and non-parallel effects are not relevant here. One is asymptotic approach in the limit $R \to \infty$ [8,9] whose accuracy cannot be verified in the present non-asymptotic study, and another one is a local approach [10] which is inconsistent for long wavelength disturbances [10] found to be preferred in the present study. Since the present formulation takes into account only systems to orders $\varepsilon$ and $\varepsilon^2$, the present results are applicable mainly to weakly nonlinear regime near the neutral stability boundary. In particular, the mean field distortion term of order $\varepsilon^3$ is not naturally taken into account here. Hence, the present formulation is similar to that used by El-Hady [4]. We pose as a solution to (8) expansions of the form

$$u_2 = \sum_{n=1}^{3} u_{2n}(y, x_s, z_s, t_s) e^{i\phi_n} + c.c. \tag{9}$$

with similar forms for $v_2$, $w_2$, etc. Substitution of these expansions into (8) and collection of coefficients of $e^{i\phi_n}$ yields

$$L_i(u_{2n}, v_{2n}, w_{2n}, \theta_{2n}, p_{2n}, \rho_{2n}) = g^i_{1n}\frac{\partial a_n}{\partial t_s} + g^i_{2n}\frac{\partial a_n}{\partial x_s} + g^i_{3n}\frac{\partial a_n}{\partial z_s} + g^i_{4n}a_n + g^i_{5n}b_n e^{-\Gamma_n}, \tag{10a}$$

where,

$$(i = 8,\ldots,13;\ \ n = 1,2,3),\ \ b_n = \overline{a_2}a_3\delta_{n1} + \overline{a_1}a_3\delta_{n2} + a_1a_2\delta_{n3},\ \ \delta_{ni} = \begin{cases} 1 \text{ for } n = i \\ 0 \text{ otherwise} \end{cases} \tag{10b}$$

$$\Gamma_1 = \int(\alpha_{3i} + \alpha_{2i} - \alpha_{1i})dx + \int(\beta_{3i} + \beta_{2i} - \beta_{1i})dz - \int(\omega_{3i} + \omega_{2i} - \omega_{1i})dt + i\chi \tag{10c}$$

$$\Gamma_2 = \int(\alpha_{3i} + \alpha_{1i} - \alpha_{2i})dx + \int(\beta_{3i} + \beta_{1i} - \beta_{2i})dz - \int(\omega_{3i} + \omega_{1i} - \omega_{2i})dt + i\chi \tag{10d}$$

$$\Gamma_3 = \int(\alpha_{1i} + \alpha_{2i} - \alpha_{3i})dx + \int(\beta_{1i} + \beta_{2i} - \beta_{3i})dz - \int(\omega_{1i} + \omega_{2i} - \omega_{3i})dt + i\chi \tag{10e}$$

$$\chi = -\int \sigma_\alpha dx_s - \int \sigma_\beta dz_s + \int \sigma_\omega dt_s \tag{10f}$$

The subscript '$i$' indicates the imaginary part, an overbar indicates complex conjugate, there is no summation convention over the subscript $n$, and the expressions for the coefficients $g^i_{mn}$ were, in general, very long [5] and will not be given here. The three systems given by (10) will have solutions only for certain right hand sides. A solution exists if and only if the corresponding solvability conditions are satisfied [11]. Applying these conditions to equations (10) lead to the following system for $a_n(n = 1,2,3)$:

$$g_{1n}\frac{\partial a_n}{\partial t_s} + g_{2n}\frac{\partial a_n}{\partial x_s} + g_{3n}\frac{\partial a_n}{\partial z_s} + g_{4n}a_n + g_{5n}b_n e^{-\Gamma_n} = 0(n = 1,2,3), \tag{11}$$

where the expressions for the coefficients $g_{mn}$ are lengthy [5] and will not be given here.

We now restrict our formulation to the special case of an infinite span wing and spatial

stability theory. There is then no dependence of the amplitude on $z$ or time $t$, and if we transform back to the fast $x$ variable we have

$$\frac{dA_n}{dx} = (G_n - \alpha_{ni})A_n + H_n^s B_n e^{is_n\psi_s} (n = 1,2,3), \tag{12a}$$

where

$$\psi_s = \varepsilon \int \sigma_3 dx, \quad H_n^s = \frac{-g_{5n}}{g_{2n}}, \quad G_n = -\varepsilon \frac{g_{4n}}{g_{2n}}, \tag{12b,c,d}$$

$$A_n = \varepsilon a_n e^{-\int \alpha_{ni} dx}, \quad s_n = \delta_{n1} + \delta_{n2} + \delta_{n3} \tag{12e,f}$$

To evaluate the nonparallel interaction coefficients, $G_n$, the slow variation in the chord wise direction of the eigenfunctions and eigenvalues must be evaluated (*i.e.* $\partial\alpha_n/\partial x_s$, $\partial u_{1n}/\partial x_s$, $\partial v_{1n}/\partial x_s$, ... *etc.* must be calculated). We differentiate the linear stability system (7) with respect to $x_s$ yielding the following system for the eigenfunctions derivatives

$$L_i\left(\frac{\partial u_{1n}}{\partial x_s}, \frac{\partial v_{1n}}{\partial x_s}, \frac{\partial w_{1n}}{\partial x_s}, \frac{\partial \theta_{1n}}{\partial x_s}, \frac{\partial p_{1n}}{\partial x_s}, \frac{\partial \rho_{1n}}{\partial x_s}\right) = g_{6n}^i \frac{\partial \alpha_n}{\partial x_s} + g_{7n}^i, \quad (i = 8,\ldots 13) \tag{13a}$$

$$\frac{\partial u_{1n}}{\partial x_s} = \frac{\partial v_{1n}}{\partial x_s} = \frac{\partial w_{1n}}{\partial x_s} = \frac{\partial \theta_{1n}}{\partial x_s} = \frac{\partial p_{1n}}{\partial x_s} = \frac{\partial \rho_{1n}}{\partial x_s} = 0 \text{ at } y = 0, \infty \tag{13b}$$

where the expressions for the coefficients $g_{6n}^i$, and $g_{7n}^i$ are lengthy [5] and will not be given here. The boundary conditions (13b) and the left side of these equations are of the same form as equations (7) which has a nontrivial solution. The system (13) therefore has a solution only if the right hand side of (13a) satisfies the solvability condition. This condition yields the value of $\partial\alpha_n/\partial x_s$. A solution of the eigenfunction derivatives is selected appropriately, as is explained in the next section, and the nonparallel coefficients are then evaluated.

Since a goal of the study is to determine the effects of compressibility for the present

problem and compare the compressible results to those of the considerably simpler incompressible counterparts, we also formulate the stability problem using the same procedure, but making use of the incompressible governing equations.

## III. NUMERICAL METHODS OF SOLUTION

The systems of equations that arise in the formulation of the triad resonance model have no analytical solution. Approximate numerical solutions to these systems have been found. There are five system types; the base flow system, the linear stability eigenvalue problem, the nonparallel system, the solvability condition, and the amplitude equations. A description of the numerical methods used to solve each of these systems follows, beginning with the base flow system.

Base Flow System

The base flow used in the calculations is that over a 23° swept infinite span wing. The airfoil section (designated SCLFC (1) - 0513F) has a normal chord of 6.44 ft. and has been extensively tested in laminar flow control experiments at NASA-Langley Research Center. The airfoil geometry is shown in figure 1. The pressure coefficient, boundary layer edge velocities, and suction distribution for the flow used in the present calculations are shown in figure 2. The suction distribution is that necessary to maintain laminar flow according to the $e^N$ criterion. These distributions as well as the boundary layer edge velocities were supplied by Dr. El-Hady of NASA-Langley Research Center for a flow with free-stream mach number of 0.82.

To obtain the base flow velocities, densities, and temperatures, we must solve the three-dimensional steady compressible boundary layer system [6] subject to the boundary layer edge and wall suction conditions supplied by Dr. El-Hady. A finite-difference code to solve just such problems has been written in Fortran by Venkit Iyer [12]. This code is fourth order accurate in the y direction (wall normal direction) and second order accurate in the x direction. The code was run on a Sun Sparcstation using a grid size of 300 nodes in the y-direction at 79 x locations concentrated near the leading edge.

Linear Stability Systems

Note first the compressible and incompressible linear stability systems are eigenvalue problems. Once $\alpha$ and $\beta$ are selected, a nontrivial solution exists only for certain values of $\omega$. Note also that the compressible system is eighth order and the incompressible system is sixth order. Thus the six velocity boundary conditions are sufficient for the incompressible system, and the eight boundary conditions (six velocity and two temperature) are adequate for the compressible system. There is no boundary condition applied to pressure or density, and the numerical discretization should not impose one.

Before discretizing the equations, we first truncate the semi-infinite domain, imposing the boundary conditions at infinity at y=50 (50 displacement thicknesses). The exact location of the truncation has been found here to have little effect on the results. The semi-infinite physical domain, approximated by y in the range $0 \le y \le 50$, is then mapped onto a computational domain for a new variable $\eta$ in the range $-1 \le \eta \le 1$, using the transformation [13]

$$\bar{\eta} = (1-c_1)(\eta^3 - c_2\eta^2 + c_2) + c_1\eta \qquad (14a)$$

$$y = c_3(1+\bar{\eta}) \Big/ \left(1 + \frac{2c_3}{50} - \bar{\eta}\right) \qquad (14b)$$

$$c_1 = \tan(30^\circ), \quad c_2 = 0.5, \quad c_3 = 1.8, \quad k = 1,... \qquad (14c,d,e)$$

We pose as approximate solutions expansions in Chebyschev polynomials as follows

$$u_{1n} = \sum_{k=0}^{N_y} a_k T_k(y), \qquad (15a)$$

where,

$$T_0(y) = 1, \quad T_1(y) = y, \quad T_{k+1}(y) = 2yT_k(y) - T_{k-1}(y), \quad k = 1,2,3,... \qquad (15b,c,d)$$

Similar expansions are used for the other velocity components and the temperature, while

expansions using one less polynomial are posed for pressure and density. The nodes for the velocity components and temperature are the Gauss-Lobatto points [13] while the pressure and density nodes are at the Gauss points. The Gauss-Lobatto points are the extrema of the last Chebyshev polynomial retained in the expansion and are given by

$$\eta_j = \cos\left(\frac{(j-1)\pi}{N_y - 1}\right), \quad j = 1,2,...N_y, \tag{16}$$

where $N_y$ is the number of collocation points. The first and last Gauss-Lobatto points lie on the boundary and are therefore suitable for application of the boundary conditions. The Gauss points are the zeros of the first neglected polynomial and lie between the Gauss-Lobatto points. Using these interior points as nodes for the pressure and density avoids the need to specify these quantities on the boundary.

In the compressible case, we have unknowns the values of the velocity components and temperature at the $N_y$ Gauss-Lobatto points and the values of pressure and density at the $N_y - 1$ Gauss points for a total of $6N_y - 2$ unknows. An equal number of equations is supplied by collocating the momentum and energy stability equations at the Gauss-Lobatto points and the continuity and state equations at the Gauss points. The base flow is interpolated from the finite-difference grid to these points by cubic spline interpolation. When such a scheme is implemented, differentiation or interpolation of functions defined on the Gauss-Lobatto or Gauss points requires only a matrix multiplication using standard matrices[5]. The six stability equations (4) collocated as specified then leads to a large system of linear algebraic equations of the form

$$\underline{\underline{M_n}}\ \underline{\varphi_{1n}} = \left[\underline{\underline{A}} - \omega_n \underline{\underline{B}}\right]\underline{\varphi_{1n}} = 0 \tag{17}$$

where $\underline{\underline{M_n}}$, $\underline{\underline{A_n}}$, and $\underline{\underline{B_n}}$ are square matrices of size $6N_y - 2$, and $\varphi_{1n}$ is a vector consisting of the values of $u_{1n}$, $v_{1n}$, $w_{1n}$, and $t_{1n}$ on the Gauss-Lobatto points and the

values of $p_{1n}$ and $\rho_{1n}$ on the Gauss points. This system is a generalized matrix eigenvalue problem which is solved for the eigenvalues using standard routines. One of these eigenvalues is selected (generally the most dangerous one) and the eigenvectors are calculated while purifying the eigenvalue by an inverse method. The eigenvalues and eigenvectors calculated by the inverse method agreed almost exactly with those calculated by the standard routine.

The incompressible case is handled in the same way. The velocity nodes are still on the Gauss-Lobatto points and the pressure is on the Gauss points. The momentum equations are collocated on the Gauss-Lobatto points and the continuity equation on the Gauss points. The system leads to a generalized eigenvalue of the same form as above, but the square matrices sizes are smaller at $4N_y - 1$. This system is solved in the same way.

Eigenvalue Search Procedure

Both the compressible and incompressible theories result in a linear stability eigenvalue problem which has a dispersion relation of the form

$$F(\alpha, \beta, \omega, R) = 0 \tag{18}$$

The real part of the frequency, $\omega_r$, of the disturbance remains constant downstream, and for the special case of spatial instabilities with zero spanwise growth rate on an infinite span swept wing considered in this analysis, $\beta_r$ is fixed as well. The chordwise wave number, $\alpha_r$, will change as the boundary layer grows, however, as will the growth rate given by $-\alpha_i$. Once the values of $\omega_r$ and $\beta_r$ are specified for a disturbance, a search for the remaining eigenvalues must be undertaken at each node of interest. A Newton-Raphson search is used to find the correct value of $\alpha$.

This Newton-Raphson method requires repetitive searches of a generalized matrix eigenvalue problem. It is possible to reduce the computer time necessary for these searches by eliminating an equation and thereby reducing the size of the matrices. This is simple in

the compressible case. Equation (7a) for $i = 13$ can be solved for $\rho_{1n}$ and substituted into equation (7a) for $i = 12$. The resulting system consists of five equations in five unknowns [5]. When this system is collocated the size of the matrices in the generalized eigenvalue problem has been reduced by approximately one sixth.

A similar reduction is applied to the incompressible system. The resulting system has the same eigenvalues as the full linear stability eigenvalue problem, but has matrices that are approximately one fourth smaller.

Solvability Condition

The second order systems, (10a), leads to solvability conditions in the form of an equation for the slowly varying amplitudes. To arrive at these conditions, we collocate the second order systems in exactly the same manner as the first order eigenvalue problem. This gives a non-homogeneous system of linear algebraic equations with the left hand side matrix identical to the first order system and therefore singular. The three systems are of the form

$$\underline{\underline{M_1}}\,\underline{\varphi_{21}} = \frac{\partial a_1}{\partial t_s}\underline{b_{11}} + \frac{\partial a_1}{\partial x_s}\underline{b_{21}} + \frac{\partial a_1}{\partial z_s}\underline{b_{31}} + a_1\underline{b_{41}} + \overline{a_2}a_3 e^{-\Gamma_1}\underline{b_{51}} \tag{19a}$$

$$\underline{\underline{M_2}}\,\underline{\varphi_{22}} = \frac{\partial a_2}{\partial t_s}\underline{b_{12}} + \frac{\partial a_2}{\partial x_s}\underline{b_{22}} + \frac{\partial a_2}{\partial z_s}\underline{b_{32}} + a_2\underline{b_{42}} + \overline{a_1}a_3 e^{-\Gamma_2}\underline{b_{52}} \tag{19b}$$

$$\underline{\underline{M_2}}\,\underline{\varphi_{23}} = \frac{\partial a_3}{\partial t_s}\underline{b_{13}} + \frac{\partial a_3}{\partial x_s}\underline{b_{23}} + \frac{\partial a_3}{\partial z_s}\underline{b_{33}} + a_3\underline{b_{43}} + a_1 a_2 e^{-\Gamma_3}\underline{b_{53}} \tag{19c}$$

Here $\underline{\varphi_{2n}}$ are vectors consisting of the values of $u_{2n}$, $v_{2n}$, $w_{2n}$, and $\theta_{2n}$ on the Gauss-Lobatto points and the values of $p_{2n}$ and $\rho_{2n}$ on the Gauss points. The vectors $\underline{b_{jn}}$ consist of the nonhomogeneous terms of the second order momentum, energy, continuity, and state equations evaluated at the appropriate Gauss-Lobatto or Gauss points.

$$\underline{b_{jn}} = \begin{bmatrix} \underline{g_{jn}^1} \\ \underline{g_{jn}^2} \\ \underline{g_{jn}^3} \\ \underline{g_{jn}^4} \\ \underline{g_{jn}^5} \\ g_{jn}^6 \end{bmatrix}, \qquad \underline{\varphi_{2n}} = \begin{bmatrix} \underline{u_{2n}} \\ \underline{v_{2n}} \\ \underline{w_{2n}} \\ \underline{\theta_{2n}} \\ \rho_{2n} \\ p_{2n} \end{bmatrix} \tag{20a,b}$$

The three systems above are linear systems of algebraic equations. Since the matrices $\underline{\underline{M_n}}$ are singular, the systems have an infinite number of solutions or no solution at all depending upon the right hand side. A solution exists for such a system if and only if the right hand side is orthogonal to the solution of the corresponding adjoint system. This solution is denoted by $\underline{x_{1n}^*}$, and the adjoint system is defined as

$$\underline{\underline{M_n^*}}\,\underline{x_{1n}^*} = 0, \text{ where } \underline{\underline{M_n^*}} \equiv \overline{\underline{\underline{M_n}}}^T. \tag{21a,b}$$

The superscript $T$ denotes transpose and the overbar indicates the complex conjugate. Applying this orthogonality condition to each of the three systems yields equations governing the variation of the amplitudes

$$g_{11}\frac{\partial a_1}{\partial t_s} + g_{21}\frac{\partial a_1}{\partial x_s} + g_{31}\frac{\partial a_1}{\partial z_s} + g_{41}a_1 + g_{51}\overline{a_2}a_3 e^{-\Gamma_1} = 0, \tag{22a}$$

$$g_{12}\frac{\partial a_2}{\partial t_s} + g_{22}\frac{\partial a_2}{\partial x_s} + g_{32}\frac{\partial a_2}{\partial z_s} + g_{42}a_2 + g_{52}\overline{a_1}a_3 e^{-\Gamma_2} = 0, \tag{22b}$$

$$g_{31}\frac{\partial a_3}{\partial t_s} + g_{32}\frac{\partial a_3}{\partial x_s} + g_{33}\frac{\partial a_3}{\partial z_s} + g_{43}a_3 + g_{53}a_1 a_2 e^{-\Gamma_3} = 0, \tag{22c}$$

where

$$g_{jn} = \underline{b_{jn}^T}\,\overline{\underline{x}}_{1n}^*. \tag{22d}$$

Nonparallel Systems

We consider first the compressible nonparallel system (13). We discretize these equations by collocating the first four on the Gauss-Labatto points and the remaining two on the Gauss points exactly as was done for the linear stability system. This yields the following set of linear algebraic equations

$$\underline{\underline{M_n}}\,\underline{\varphi_n^{NP}} = \frac{\partial \alpha_n}{\partial x_s}\underline{b_{6n}} + \underline{b_{7n}} \tag{23}$$

Here $\underline{\varphi_n^{NP}}$ is a vector consisting of the values of $\partial u_{1n}/\partial x_s$, $\partial v_{1n}/\partial x_s$, $\partial w_{1n}/\partial x_s$, and $\partial \theta_{1n}/\partial x_s$ at the Gauss-Labatto points and the values of $\partial \rho_{1n}/\partial x_s$, and $\partial p_{1n}/\partial x_s$ at the Gauss points. The vectors $\underline{b_{jn}}$ consist of the nonhomogeneous terms of the nonparallel system evaluated at the appropriate Gauss-Labatto or Gauss points.

$$\underline{b_{jn}} = \begin{bmatrix} g_{jn}^1 \\ g_{jn}^2 \\ g_{jn}^3 \\ g_{jn}^4 \\ g_{jn}^5 \\ g_{jn}^6 \end{bmatrix} \qquad \underline{\varphi_n^{NP}} = \begin{bmatrix} \partial u_{1n}/\partial x_s \\ \partial v_{1n}/\partial x_s \\ \partial w_{1n}/\partial x_s \\ \partial \theta_{1n}/\partial x_s \\ \partial \rho_{1n}/\partial x_s \\ \partial p_{1n}/\partial x_s \end{bmatrix} \tag{24a,b}$$

Since the matrices $\underline{\underline{M_n}}$ are singular, a solution exists for such a system if and only if the right hand side is orthogonal to the solution of the corresponding adjoint system. This condition yields

$$\frac{\partial \alpha_n}{\partial x_s} = -\frac{g_{7n}}{g_{6n}} \tag{25a}$$

where,

$$g_{jn} = \underline{b_{jn}^T}\,\underline{\overline{x}_{1n}^*}. \tag{25b}$$

With this value of $\partial \alpha_n/\partial x_s$, an infinite number of solutions exist since their is a nontrivial

solution to the homogeneous problem. A procedure known as the method of least squares [14] exists which will find the solution which has minimum $\|\cdot\|_2$ norm. It makes use of the singular value decomposition of the matrix $M$ into a product of three matrices as follows

$$\underline{\underline{M_n}} = \underline{\underline{U_n}}\,\underline{\underline{\Sigma_n}}\,\underline{\underline{V_n^T}}. \tag{26}$$

The matrix $\underline{\underline{\Sigma_n}}$ consists of the singular values, $\sigma_j$, of the matrix $\underline{\underline{M_n}}$ on the diagonals and zeros off the diagonal. The three decomposition matrices are calculated using a standard IMSL routine. The least squares solution with minimum norm is then given by

$$\underline{\tilde{\varphi}_n^{NP}} = \underline{\underline{V_n}}\,\underline{y} \tag{27a}$$

where,

$$y_j = \begin{cases} b_j/\sigma_j & j=1,\ldots k \left(k \text{ is the rank of } \underline{\underline{M_n}}\right) \\ 0 & \text{other } j \end{cases} \tag{27b}$$

$$\underline{b_j} = \underline{\underline{U_n^T}}\,\underline{b}. \tag{27c}$$

The general solution of the nonparallel system then is

$$\underline{\varphi_n^{NP}} = \underline{\tilde{\varphi}_n^{NP}} + c\underline{\varphi_{1n}} \tag{28}$$

where $c$ is an arbitrary constant. We select a specific solution by requiring that the non-parallel solution be orthogonal to the linear stability solution. The solution is found by subtracting the component of the least squares solution that is not normal to the linear stability solution

$$\underline{\varphi_n^{NP}} = \underline{\tilde{\varphi}_n^{NP}} - \underline{\tilde{\varphi}_n^{NP}} \cdot \underline{\varphi_{1n}}, \tag{29a}$$

where the inner product is defined as

$$\underline{a} \cdot \underline{b} = \underline{b^T \bar{a}}. \tag{29b}$$

Note that with this particular solution of the nonparallel solution

$$\underline{\varphi_n^{NP}} \cdot \underline{\varphi_{1n}} = \frac{\partial \underline{\varphi_{1n}}}{\partial x_s} \cdot \underline{\varphi_{1n}} = \frac{1}{2}\frac{\partial}{\partial x_s}\left(\underline{\varphi_{1n}} \cdot \underline{\varphi_{1n}}\right) = \frac{1}{2}\frac{\partial}{\partial x_s}\left(\left\|\underline{\varphi_{1n}}\right\|_2^2\right) = 0, \tag{30}$$

so we see that the magnitude of the vector of eigenfunctions does not change magnitude as we move downstream. This is a desirable quality, since the size of the disturbance is then indicated by the amplitude, $A_n$, alone. If the eigenvector magnitude were allowed to change, the disturbance size would be indicated by the product of the amplitude and the eigenfunction magnitude.

Normalization of the Eigenfunctions

The linear growth rate and nonparallel coefficient are independent of the normalization of the eigenfunctions, but the interaction coefficients are not. To make the interaction coefficients unique, we normalize the eigenfunctions according to the following procedure. At the first node calculated, each of the three eigenfunctions is normalized such that the maximum magnitude of $u_{1n}$ in the interval $0 \le y \le \infty$ is one. The derivatives of the eigenfunctions with respect to $x_s$, is then obtained by solving the nonparallel system. The eigenfunctions at the next downstream node are predicted from these derivatives using finite differences. Central differencing is used except following the first node where it is impossible to do so. The linear stability system is then solved at the next node and the eigenfunctions normalized for the moment by again requiring the maximum magnitude of $u_{1n}$ to be one. Let the vector containing these eigenfunctions be denoted $\underline{\varphi_n}$, and call the predicted eigenfunction vector $\underline{\varphi_n^{pred}}$. We wish to select the normalization constant $C = C_r + iC_I$ so as to minimize the difference between the predicted and actual eigenfunction. Let the difference vector, $\underline{E}$, be defined as

$$\underline{E} = C\underline{\varphi_n} - \underline{\varphi_n^{pred}}. \tag{31}$$

The square of the difference vector magnitude is then given by

$$\|\underline{E}\|_2^2 = \sum_j \left\{ \left( C_r \phi_{rj} - C_i \varphi_{ij} - \varphi_{rj}^{pred} \right)^2 + \left( C_r \phi_{ij} + C_i \varphi_{rj} - \phi_{ij}^{pred} \right)^2 \right\} \tag{32}$$

where $\varphi_{rj}$ and $\varphi_{ij}$ indicate the real and imaginary part of the jth element of the vector $\underline{\varphi_n}$ and a similar meaning applies for the predicted vector symbols. To find the constant $C$ that minimizes this quantity, the partial derivatives are set to zero.

$$\frac{\partial \|\underline{E}\|_2^2}{\partial C_r} = \sum_j \left\{ 2\left( C_r \varphi_{rj} - C_i \varphi_{ij} - \varphi_{rj}^{pred} \right) \varphi_{rj} + 2\left( C_r \varphi_{ij} - C_i \varphi_{rj} - \varphi_{ij}^{pred} \right) \varphi_{ij} \right\} = 0 \tag{33a}$$

$$\frac{\partial \|\underline{E}\|_2^2}{\partial C_i} = \sum_j \left\{ 2\left( C_r \varphi_{rj} - C_i \varphi_{ij} - \varphi_{rj}^{pred} \right) \varphi_{rj} + 2\left( C_r \varphi_{ij} - C_i \varphi_{rj} - \varphi_{ij}^{pred} \right) \varphi_{ij} \right\} = 0 \tag{33b}$$

Solving these equations simultaneously yields

$$C_r = \frac{\sum_j \left( \varphi_{rj} \varphi_{rj}^{pred} + \varphi_{ij} \varphi_{ij}^{pred} \right)}{\sum_j \left( \varphi_{rj}^2 + \varphi_{ij}^2 \right)}, \qquad C_i = \frac{\sum_j \left( \varphi_{rj} \varphi_{ij}^{pred} - \varphi_{ij} \varphi_{rj}^{pred} \right)}{\sum_j \left( \varphi_{rj}^2 + \varphi_{ij}^2 \right)}. \tag{34a,b}$$

The normalized eigenvector, then, is given by

$$\underline{\varphi_{1n}} = C \underline{\varphi_n} \,. \tag{35}$$

Integration of the Amplitude Equations

The evolution of the disturbance amplitudes in space can be obtained by integrating the spatial theory amplitude equations which are of the following form for both the incompressible and compressible theories.

$$\frac{dA_1}{dx} = \left( G_1 - \alpha_{1i} \right) A_1 + H_1^s \overline{A}_2 A_3 e^{i\psi} \tag{36a}$$

$$\frac{dA_2}{dx} = (G_2 - \alpha_{2i})A_2 + H_2^s \overline{A}_1 A_3 e^{i\psi} \tag{36b}$$

$$\frac{dA_3}{dx} = (G_3 - \alpha_{3i})A_3 + H_3^s A_1 A_2 e^{-i\psi} \tag{36c}$$

These amplitude equations are complex. To obtain real equations for the amplitudes and phases we let

$$A_n = A_n^* e^{i\delta_n} \tag{37a}$$

$$G_n = G_n^* e^{i\chi_n} \tag{37b}$$

$$H_n = H_n^* e^{i\tau_n}. \tag{37c}$$

On substitution into the complex amplitude equations and removal of the asterisks, we have

$$\frac{dA_1}{dx} = (G_1 \cos\chi_1 - \alpha_{1i})A_1 + \frac{1}{2}H_1 A_2 A_3 \cos(\gamma + \tau_1 + \psi) \tag{38a}$$

$$\frac{dA_2}{dx} = (G_2 \cos\chi_2 - \alpha_{2i})A_2 + \frac{1}{2}H_2 A_1 A_3 \cos(\gamma + \tau_2 + \psi) \tag{38b}$$

$$\frac{dA_3}{dx} = (G_3 \cos\chi_3 - \alpha_{3i})A_3 + \frac{1}{2}H_3 A_1 A_2 \cos(-\gamma + \tau_3 + \psi) \tag{38c}$$

$$\frac{d\gamma}{dx} = (G_3 \sin\chi_3 - G_2 \sin\chi_2 - G_1 \sin\chi_1) + H_3 \frac{A_1 A_2}{2A_3}\sin(-\gamma + \tau_3 - \psi)$$

$$-H_2 \frac{A_1 A_3}{2A_2}\sin(\gamma + \tau_2 + \psi) - H_1 \frac{A_2 A_3}{2A_1}\sin(\gamma + \tau_1 + \psi) \tag{38d}$$

where,

$$\gamma = \delta_3 - \delta_2 - \delta_1 \tag{38e}$$

With initial values, $A_{n0}$ and $\gamma(0)$ of the amplitudes $(A_n, n = 1,2,3)$ and phase difference $(\gamma)$ specified, we integrate these equations using a standard fourth-order variable interval

Runge-Kutta method. When the Runge-Kutta method requires values of the interaction coefficients between nodes of the linear stability calculations, we make use of cubic spline interpolation to obtain them. Finally, we define the $N$-factor as

$$N = ln(A_n / A_{n0}). \tag{39}$$

In the next section we present the results which are based on disturbances of size $\varepsilon$ which can lead to maximum $N$ factor of about 7, while in real transition $N$ can approach value about 10 or so.

## IV. RESULTS

We consider here the effect of the nonlinear resonant wave interaction on the $N$-factors of the members of the triad. Triads consisting of different combinations of Tollmien-Schlichting (TS), and crossflow (CF), modes are examined. In specifying the eigenvalues of these modes, the spanwise wave numbers, $\beta_n$, have been made non-dimensional using a reference length of $1.0 \times 10^{-4} m$, and the frequencies, $\omega_n$, were non-dimensionalized using a reference time of $3.333 \times 10^{-7} s$. The chord wise wavenumbers, $\alpha_n$, change as they move downstream, so only the approximate wave angles, $\psi_n$ are specified.

TS-TS-TS Triad

First we study a triad composed of three TS modes. The triad has frequencies, $\omega_1 = 0.05015$, $\omega_2 = -0.02929$, and $\omega_3 = 0.02086$. The spanwise wavenumbers are $\beta_1 = 0.06$, $\beta_2 = 0.04$, and $\beta_3 = 0.10$. These frequencies and spanwise wavenumbers satisfy the resonant conditions exactly at all streamwise locations. The chordwise wave numbers are shown in figure 3. Note that this triad is substantially detuned as seen by comparing the sum, $\alpha_1 + \alpha_2$, to $\alpha_3$. Calculations begin at $R = 1612$ just before the location where modes 2 and 3 begin to grow. The linear parallel growth of these modes is determined. The first mode grows rapidly before beginning an equally rapid decay. The

second and third modes decay initially before beginning a steady growth over the entire region calculated. The third mode is very weakly unstable according to the linear theory.

We consider the case $\varepsilon_1 << \varepsilon$ first, and only examine the nonlinear evolution of the triad amplitudes. The nonlinear interaction coefficients are shown in figure 4. Note the very large magnitude of the TS3 interaction coefficient and the substantial TS2 coefficient, while the TS1 coefficient is very near zero. This indicates that the 2nd and 3rd modes are more susceptible to effects of the interaction. We then determined the nonlinear growth of modes two and three with initial amplitudes of A10=A20=1.OE-5 for various initial amplitudes of mode 1. The results indicate that when all three modes have the same small initial amplitude, the interaction is very weak. As the initial amplitude of the first mode is increased, the other two modes show greater deviation from their linear results. Note that the effect on mode three is found to be more dramatic than the effect on mode two because of its larger interaction coefficient. In each of these cases there was no effect at all on mode 1. The phase difference, $\gamma$, for some of these calculations is also determined. Little deviation from the linear results $(\gamma = \pi = \text{constant})$ was found for very small initial amplitudes as expected. For larger amplitudes, however, the phase difference changes substantially, especially downstream some distance, where the amplitudes have developed sufficiently to interact strongly.

A larger initial amplitude of the second mode was found to affect the third. Note in this case that the third mode is dramatically affected, while the second mode is too much larger than the others to be affected at all. The 1st mode is initially small like the 3rd, but is still unaffected because of its small interaction coefficient.

If both the first and third mode are much larger than the second, the interaction can dramatically affect the second. This is shown in figure 5. Note in this figure that the third mode was also substantially affected, while the first mode with the same initial amplitude as the third showed no deviation at all (not shown). The third mode's small interaction coefficient apparently makes it resistant to the effects of the triad interaction. Our further

results, which indicated the growth of the modes when the first mode is 100 times smaller than the other two, offers further support for this conclusion. The first mode shows very little deviation from its linear growth despite its relatively small initial size.

Generally, the $N$-factor of a mode is more strongly affected when that mode is smaller than the other members of the triad. How much smaller the mode needs to be depends upon the amplitude of the other two modes. Our other results indicated the growth of the third TS mode when its initial amplitude is one tenth the size of the other two. Note that for small amplitudes, the nonlinear interaction is negligible and the linear stability theory is adequate. As the amplitudes increase in size, however, nonlinearity is found to have a powerful effect on the growth of the TS3 mode. If the initial amplitudes of the modes are sufficiently high, a powerful interaction is found to occur even when the modes are initially the same size.

The initial phase difference also plays an important role in the development of the disturbance amplitudes. We found the growth of the three modes for a number of initial phase differences. The 1st mode, however, did not deviate from its linear growth in every case. The linear theory predicts consistent slow growth for the third mode. The nonlinear theory shows consistent nonlinear growth for some initial phases, while for others, the third mode actually decays substantially before beginning to grow. In each case, however, the third mode is eventually destabilized substantially by the interaction. The 2nd mode is affected in each case as well.

The imperfect tuning of this triad has an effect on the interaction as well. We found the growth of the third mode with the actual tuning and with "perfect" tuning. The "perfect" tuning results were obtained by setting the detuning parameter to zero at each streamwise location. The imperfect tuning weakens the interaction in the case considered, and the evolution of the phase difference is affected as well.

TS-TS-CF Triad

We now consider a triad composed of two TS and one CF mode. The triad has

frequencies, $\omega_1 = -0.02743$, $\omega_2 = 0.02821$, and $\omega_3 = 0.00078$. We were not successful to find a stationary CF mode that can form a triad. However, the CF mode considered here has a very small frequency. The spanwise wavenumbers are $\beta_1 = 0.02$, $\beta_2 = 0.06$, and $\beta_3 = 0.08$. These frequencies and spanwise wavenumbers satisfy the resonant conditions exactly at all streamwise locations. The chordwise wavenumbers are shown in figure 6. This triad is well tuned, much more so than the TS-TS-TS triad. Calculations begin at $R = 139$ where the third (crossflow) mode begins to grow. The linear parallel growth of these modes was determined. The two TS modes grow rapidly before stabilizing, while the crossflow mode grows very weakly before beginning a very slow decay.

The spatial interaction coefficients for this triad are shown in figure 7. The crossflow mode has a very large interaction coefficient, while both TS modes have coefficients very near zero (on the order of $10^{-2}$). The spatial development of the crossflow mode was determined and is shown in figure 8 for several different initial crossflow mode amplitudes with the initial amplitudes of the TS modes equal and fixed. The crossflow mode shows strong nonlinear growth even when its initial amplitude is the same size as the TS modes. When the crossflow mode is substantially smaller, the interaction is even more destabilizing. The TS modes, however, do not vary from their linear growth in any of the cases shown, presumably because of their very low interaction coefficients.

It is possible for one of the TS modes to be affected by the interaction, given the proper distribution of initial amplitudes. Large amplitudes of the other two modes, combined with a much smaller TS mode amplitude is required. We found an effected TS1 mode and an effected TS2 mode. The initial amplitudes required to cause the nonlinear TS mode growth, as determined from our calculation, seems unlikely when the very small CF growth rate and much larger TS mode growth rates are considered.

The effect of the initial phase difference on the nonlinear growth of the CF mode was also determined. The effect of the initial phase is similar to the effect in the TS-TS-TS

triad. For some initial phase differences, the CF amplitude initially falls, while for others CF growth is immediate. In every case, however, the CF mode eventually begins to grow rapidly. Far downstream, the amplitude is about the same for each of the initial phases tested. Apparently, the initial decay in some of the cases is made up for by extra strong growth downstream due to the smaller amplitude. In each case shown, the two TS modes were not affected by the interaction due to their small interaction coefficients.

TS-CF-CF Triad

The chordwise wavenumbers for a triad consisting of one TS mode and two CF modes are shown in figure 9. No steady CF is found to form a triad in this case and, thus, the triad considered here consists of traveling modes only. The triad has frequencies, $\omega_1 = -0.1737$, $\omega_2 = 0.01401$, and $\omega_3 = -0.00336$. The spanwise wavenumbers are $\beta_1 = 0.21$, $\beta_2 = 0.17$, and $\beta_3 = 0.38$. These frequencies and spanwise wavenumbers satisfy the resonant conditions exactly at all streamwise locations. The tuning of the chordwise wavenumbers is imperfect, however, as shown in figure 9. The linear growth of the three modes is determined and indicated that the two crossflow modes are weakly unstable, while the TS mode is damped substantially.

The nonlinear behavior of this triad is influenced by the spatial interaction coefficients shown in figure 10. The TS mode has a very small coefficient, while the CF coefficients are order 1 but still much smaller than the CF coefficient in the TS-TS-CF triad. Despite the order one CF interaction coefficients, nonlinear growth of a CF mode occurs only when the initial amplitude of that mode is much smaller than the other two. The rapid decay of the TS mode quickly makes it too small to significantly affect a CF mode. Figure 11 shows the linear and nonlinear growth of the triad amplitude when the third CF modes initial amplitude is relatively small. The CF2 mode and the TS1 modes are unaffected by the interaction while the CF3 mode shows only weak deviation from linear theory despite its much smaller amplitude.

The decay of the TS1 mode seems to be the dominating influence on the triad. Our

other results indicated the triad evolution when all three modes have equal initial amplitude. The two crossflow modes do not deviate from linear theory, despite their large interaction coefficients. The TS mode, with a very small interaction coefficient, decays according to linear theory until its amplitude becomes much smaller than the CF modes. Nonlinear effects then cause it to decay even more rapidly than linear theory predicts. If the initial amplitudes of all three modes are made ten times bigger, the interaction is stronger as one would expect. We also determined the triads evolution under these circumstances. The third CF mode begins to show very slight nonlinear deviation while the CF2 mode is still unaffected. The TS mode decays linearly again for a short distance before showing nonlinear effects. Interestingly, with the same initial phase but larger initial amplitudes, nonlinearity causes growth in this case rather than decay. The behavior of the triad amplitudes apparently depends strongly upon the initial amplitudes.

CF-CF-CF Triad

Consider now a triad consisting of three CF modes with frequencies, $\omega_1 = 0.002139$, $\omega_2 = .000395$, and $\omega_3 = 0.002534$ and spanwise wavenumbers $\beta_1 = 0.10$, $\beta_2 = 0.10$, and $\beta_3 = 0.20$. No steady CF is found to form a triad in this case and thus, the triad considered here consists of traveling modes only. These frequencies and spanwise wavenumbers satisfy the resonant conditions exactly at all streamwise locations. The tuning of the chordwise wavenumbers is shown in figure 12. The linear growth of the third CF mode is found to be stronger than the other two. The calculations begin at a Reynolds number of 1317 where the first CF mode first becomes unstable.

The nonlinear evolution of the triad is characterized by the spatial interaction coefficients shown in figure 13. All three coefficients are quite small with none of them exceeding 0.04. The third modes interaction coefficients falls to an especially small magnitude downstream. The growth of the second mode for a number of its initial amplitudes with fixed values of the first and third modes is determined. When the initial amplitude is the same size as the other two, there is very little deviation from linear theory.

When it's one tenth the size, the deviation is still small. Smaller initial values begin to cause more significant nonlinear growth. There was no substantial nonlinear effect on modes one and three in each of the cases considered. Larger initial values of the first and third modes still show only small nonlinear effects when the initial amplitudes are of the same size. This is shown in figure 14 where the initial amplitudes are relatively large. At these large amplitudes, however, the interactions effect on the growth of the second mode becomes strong if the second mode is initially smaller as shown. We were not able to find CF-CF-CF triads that linearly give high $N$ factor, otherwise we could have obtained results for the nonlinear $N$ factor considerably higher than those shown in figure 14.

The effect of the initial phase difference on the growth of the second mode when it is significantly smaller than the other two is also determined. The initial phase difference strongly affects the early behavior of this mode. The interaction causes a sharp decline in amplitude for some initial values and sharp growth for others. It is interesting to note, however, that the mode's amplitude recovers from the initial decline, and far downstream the amplitude is nearly the same for each case.

Nonparallel Effects

We examine now the effects that nonparallelism of the boundary layer has upon the evolution of the triad amplitudes for $\varepsilon_1 \equiv \varepsilon$. Figure 15 shows the parallel and nonparallel growth of the three modes making up the TS-TS-TS triad considered before. The effect of the boundary layer growth is destabilizing to all three TS modes. The nonlinear evolution of the third mode for the nonparallel case is compared to the parallel case in figure 16. The nonlinear effects are quite similar in the parallel and nonparallel cases, although the $N$ factors are made larger by the destabilizing effect of the boundary layer growth. The initial growth is dominated by the nonparallel effect until the modes reach sufficient amplitude to react nonlinearly. It should be noted that associated with the destabilizing effect of non-parallelism there is, in general, also stabilizing effect of curvature. However, in the present weakly nonlinear and nonparallel problem $(\varepsilon_1 \le \varepsilon << 1)$ with neglected $0(\varepsilon^n)(n \ge 3)$

effects, curvature terms alone are at most of order $\varepsilon\varepsilon_1^2$ and, thus, are not included in the analysis.

The growth of the crossflow mode in the TS-Ts-TS triad is considered in figure 17. Nonparallel effects are seen to be strongly destabilizing to the crossflow mode. Nonlinear effects, however, are slightly less dramatic in the nonparallel case. This is simply due to the nonparallel effects making the amplitude of the crossflow mode larger making it less susceptible to the effects of the TS modes. Nonparallel effects also make the TS modes larger, but less so than it does for the CF mode. Once again nonparallel effects are dominant early while the amplitudes are still too small to interact strongly. In fact, the nonlinear growth is identical to the nonparallel linear growth for some distance.

The growth of the first and second mode in the CF-CF-CF triad are determined and the first mode is shown in figure 18. Nonlinear effects on this triad are generally weak despite the rather large initial amplitudes because of the small interaction coefficients. The growth once again is dominated by nonparallel effects until near the end of the calculated region as seen in the figure. Here, the amplitudes have presumably reached such large magnitudes that nonlinear growth occurs despite the weakness of the interaction. Note that in the parallel case, the amplitudes never reach sufficient size for an appreciable interaction to take place. So in a sense, nonparallel effects strengthen the interaction in that they boost the linear growth of the modes creating large enough amplitudes to interact nonlinearly.

The Incompressible Theory

It is often the practice to make use of the incompressible theory even in a compressible flow because of the savings in calculation time. The incompressible theory in many cases give similar results to the compressible case. We examine now the usefulness of the incompressible theory in the triad interaction case.

Figure 19 compares the compressible and incompressible interaction coefficients for the TS-TS-TS triad considered previously. Both theories show a large coefficient for the third mode, a very small coefficient for the first mode, and an intermediate value for the

second. The incompressible theory, however, overpredicts the magnitude of all three interaction coefficients by more than a factor of two at many values of the Reynolds number. This over prediction, coupled with the larger linear growth rates of the incompressible theory, substantially affects the evolution of the triad amplitudes. Figure 20 compares the incompressible and compressible evolution of the third mode. The incompressible theory shows a very strong destabilizing effect on the third mode while the compressible theory shows a weak interaction. The difference is likely due to the incompressible theory's faster linear growth of the TS1 and TS2 modes, which creates larger amplitudes to affect the third mode. The larger incompressible interaction coefficients further strengthen the interaction. The incompressible theory clearly is not an adequate predictor of the magnitude of the interaction coefficient for this TS-TS-TS triad, but it does correctly predict large coefficients for modes two and three and a very small one for mode one.

The compressible and incompressible interaction coefficients for the TS-TS-CF triad previously considered are shown in figure 21. The incompressible theory agrees well with the compressible theory on the crossflow mode's interaction coefficient, although the incompressible theory is slightly high. Both theories show the TS1 and TS2 coefficients to be quite small, but the incompressible theory again overpredicts them by more than a factor of two. Figure 22 shows the spatial evolution of the third mode for the initial conditions shown. The incompressible theory again shows a much stronger interaction than the compressible theory. This again is due to the higher linear growth of the TS modes as well as the larger incompressible interaction coefficient.

The interaction coefficients for a CF-CF-CF triad are shown in figure 23. Both the incompressible and compressible theories predict the coefficients for all three modes to be very small. The incompressible theory overpredicts the interaction coefficient magnitudes, but only slightly. The evolution of the second mode when its initial amplitude is smaller than the other two is shown in figure 24. The nonlinear effect is stronger in the

incompressible case due to the larger linear growth rates as well as a larger interaction coefficient.

## V. Discussion

The present results indicate that the magnitude of a mode's interaction coefficient coupled with the initial spectrum of amplitudes and phases govern its nonlinear growth as a member of a resonant triad. If its interaction coefficient is small, the mode's amplitude may be boosted only if it is much smaller than the amplitudes of the other two members. With a larger interaction coefficient, a mode's amplitude may be boosted even when the same size as its fellow triad members.

The interaction coefficients of four different types of triads consisting of different combinations of TS and CF modes are presented in the present paper. Calculations of the interaction coefficients for many different triads of each of these four types show the same pattern as those presented [5]. That is, combinations of three crossflow modes (CF-CF-CF) whose wavenumbers satisfy the triad resonance conditions show very small interaction coefficients for all three members. TS-TS-CF triads show a very strong crossflow interaction coefficient and very small TS coefficients. The TS-CF-CF and TS-TS-TS combinations also show the same pattern as the triads of the same type presented in this paper, although these type of triads are relatively rare on the wing used in this study.

Without knowledge of these results, the most likely wave interaction scenario would involve a crossflow mode whose amplitude had grown large as it approached the TS instability region. The growth of smaller amplitude TS modes might then be boosted by a triad interaction. The present results, however, indicate that the TS interaction coefficients are very small, and this type of interaction would be relatively weak. Instead, the very large CF interaction coefficient in the TS-TS-CF triad indicates that a small amplitude CF mode may be boosted after the TS modes have reached some finite amplitude.

The simpler incompressible theory yields interaction coefficients with the same pattern as the compressible theory, but the magnitudes of the interaction coefficients differ

substantially for some triads. This difference, coupled with the higher incompressible linear growth rate causes nonlinear effects to be overestimated. Hence, the popular and convenient incompressible modeling assumption may not yield meaningful results for subsonic compressible flows such as the one investigated in this paper.

The predictions of this theory differ in important ways from the parametric resonance theory introduced by Herbert [15] and extended to 3-D flows by Reed [16] and Fischer and Dallman [17]. The parametric approach considers the linear growth of infinitesimal secondary instabilities in a flow consisting of finite amplitude primary waves superposed upon the base flow. These theories generally show a primary threshold amplitude of a few percent, below which there is no secondary instability. The resonant theory presented in this paper, however, shows significant interactions among disturbances at much smaller amplitudes. The resonant wave interaction theory may be the better model in the early stages of transition before disturbances have reached the threshold amplitude for secondary instability. It may also be more appropriate on laminar flow control wings where the amplitudes of disturbances are kept small.

El-Hady [4] derives expressions for the interaction coefficients using an incompressible model. His expressions for interaction coefficients are equivalent to those of the present model for the incompressible case. The results he presents for a few triads in the same flow do not match the pattern of the present calculations, however. The linear stability results of El-Hady and the present calculations match very well. The nonparallel coefficients, which make use of a solvability condition but do not depend upon eigenfunction normalization, also match well. The difference in the interaction coefficients is therefore likely due to differing eigenfunction normalizations. The present calculations sets the eigenfunction magnitude of all three members to one, and then preserves the eigenfunctions magnitudes downstream. The physical disturbance's amplitude is therefore indicated by A only, rather than the product of A and the eigenfunction magnitude. Normalization schemes that do not set the magnitudes of all three eigenfunctions to the

same size, or allow changes in eigenfunction magnitude downstream, may result in very different interaction coefficients.

**Acknowledgment**

This work was supported in part by the National Center for Supercomputing Applications. The authors also would like to thank Dr. Nabil El-Hady for information regarding wing geometry and pressure coefficient data.

## References


1. A. D. D. Craik. Non-linear resonant instability in boundary layers, *Journal of Fluid Mechanics* **50**, 393-413 (1971).

2. A. D. D. Craik. Wave interactions and fluid flows, (Cambridge University Press, Cambridge, 1985).

3. S. G. Lekoudis. Resonant wave interactions on a swept wing, *AIAA Journal* **18**, 122-124 (1980).

4. N. M. El-Hady. Evolution of resonant wave triads in three-dimensional boundary layers, *Physics of Fluids A* **1**, 549-563, (1989).

5. M. P. Vonderwell. Wave interactions in three-dimensional boundary layers, Ph.D. Dissertation, University of Illinois, Urbana, Illinois (1994).

6. H. Schlichting. Boundary Layer Theory, 7th ed. (McGraw-Hill Co., New York, 1979).

7. F. M. White. Viscous fluid flow, 2nd ed. (McGraw-Hill Co., New York, 1991).

8. F. T. Smith. On the nonparallel flow stability of the Blasius boundary layer, *Proceedings of the Royal Society London A* **366**, 91-109 (1979).

9. M. E. Goldstien, and P. A. Durbin. Nonlinear critical layers eliminate the upper branch of spatially growing Tollmien-Schlichting waves, *Physics of Fluids* **29**, 2344-2345 (1986).

10. F. P. Bertolotti, T. Herbert, and P. R. Spalart. Linear and nonlinear stability of the Blasius boundary layer, *Journal of Fluid Mechanics* **242**, 441-474 (1992).

11. P. G. Drazin, and W. H. Reid. Hydrodynamic Stability, 1st ed. (Cambridge University Press, Cambridge, UK, 1980).

12. V. Iyer. Computation of three-dimensional compressible boundary layers to fourth-order accuracy on wings and fuselages, NASA Contractor Report 4269, 1-222 (1990).

13. S. Balachandar, C. L. Streett, and M. R Malik. Secondary instability in rotating disk flow, AIAA-90-1527 (1990).

14. B. Noble, and J. Daniel. Applied linear algebra, 2nd ed. (Prentice-Hall Inc., Englewood Cliffs, New Jersey, 1977).

15. T. Herbert. Three-dimensional phenomenon in the transitional flat plate boundary layers, AIAA paper no. 85-0489 (1984).

16. H. Reed. Wave interactions in swept-wing flows, AIAA paper no. 84-1678 (1984).

17. T. M. Fischer, and U. Dallman. Theoretical investigation of secondary instability of three-dimensional boundary layer flows, AIAA paper no. 84-0009 (1984).

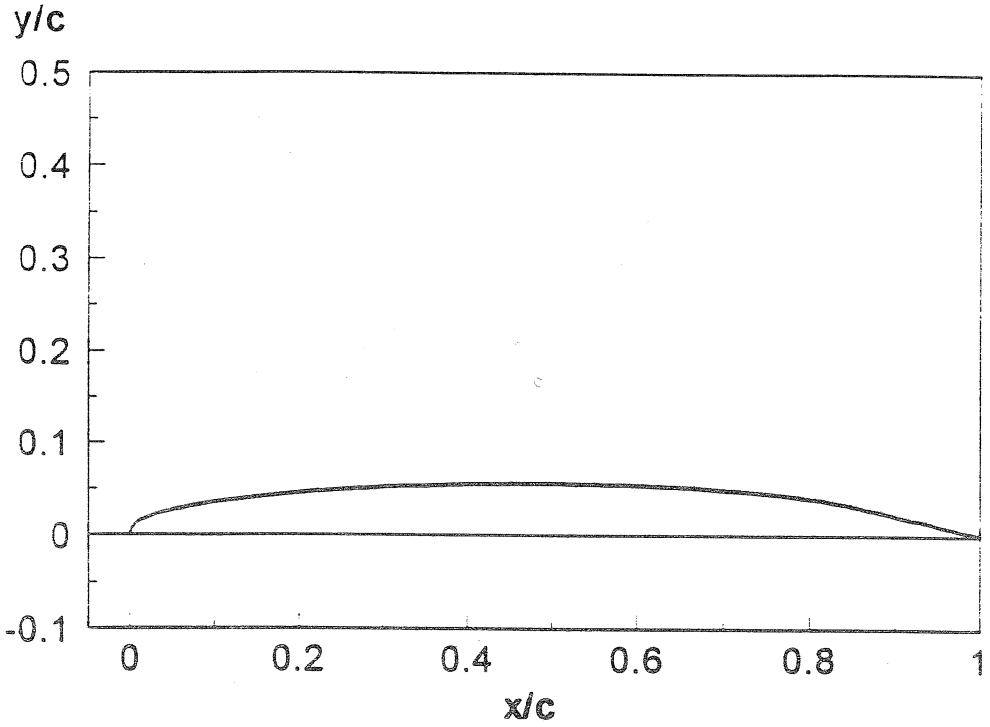


Figure 1: Shape of the top surface of the wing.

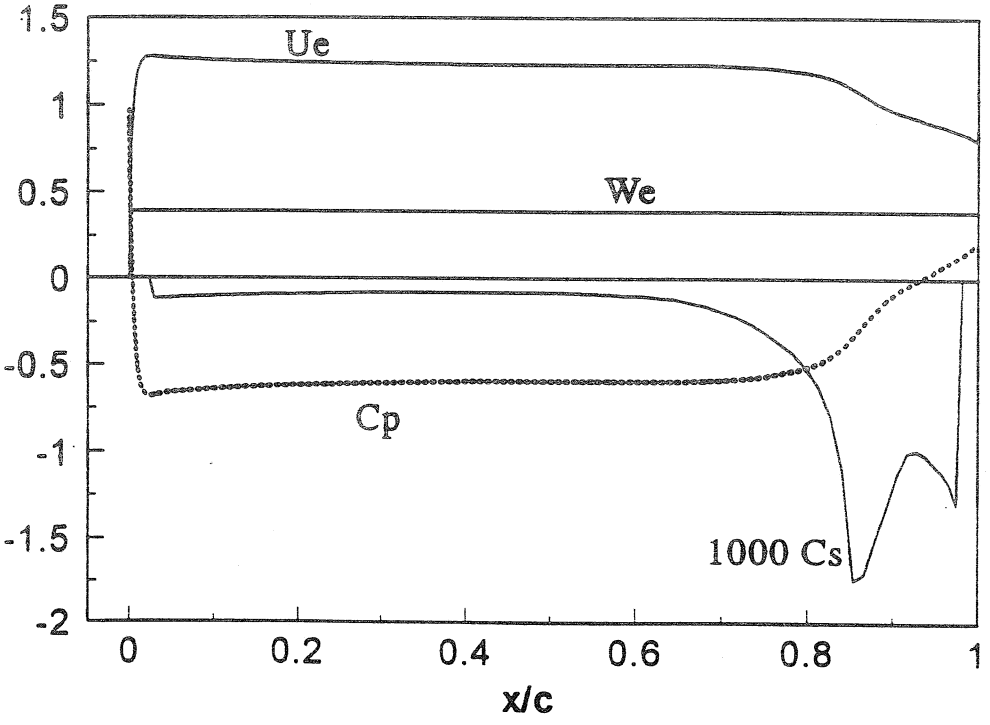


Figure 2: Coefficient of pressure, $C_p$, suction coefficient.

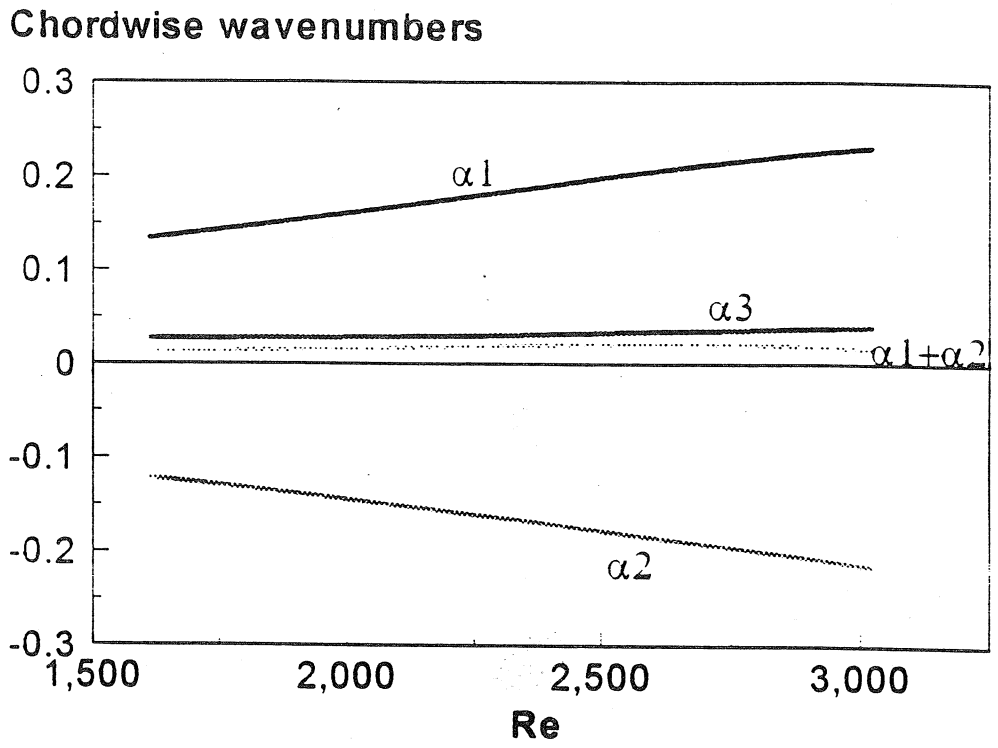


Figure 3: Compressible chordwise wavenumbers for a TS-TS-TS triad and the sum of the first two.

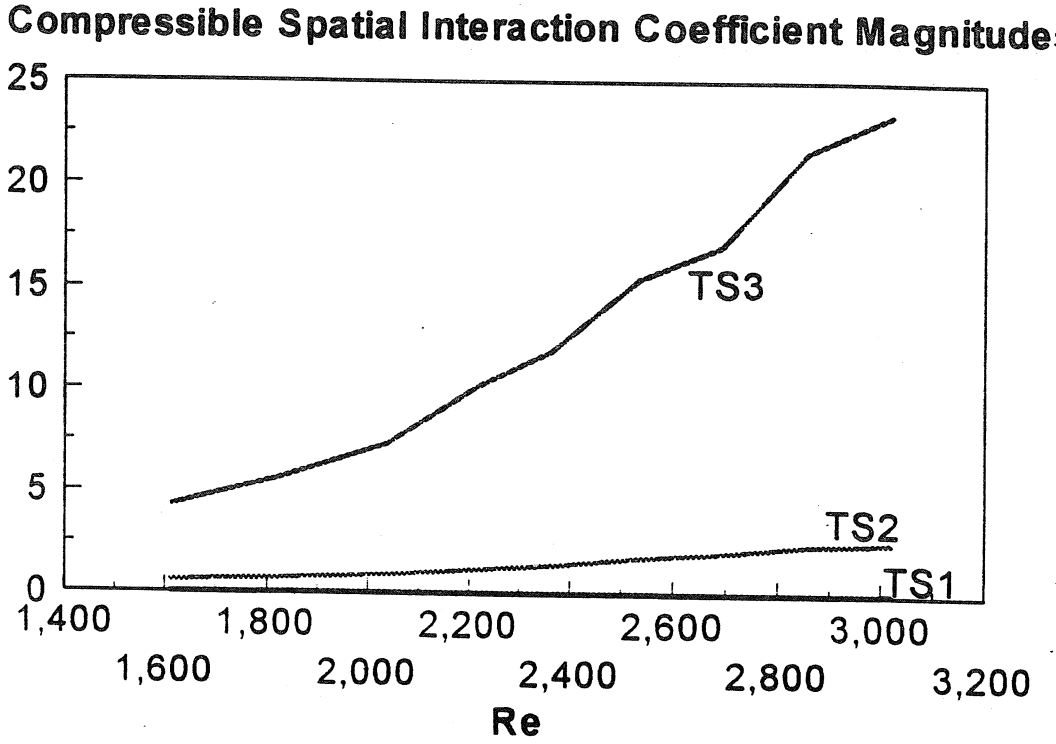


Figure 4: Compressible spatial interaction coefficients for a TS-TS-TS triad.

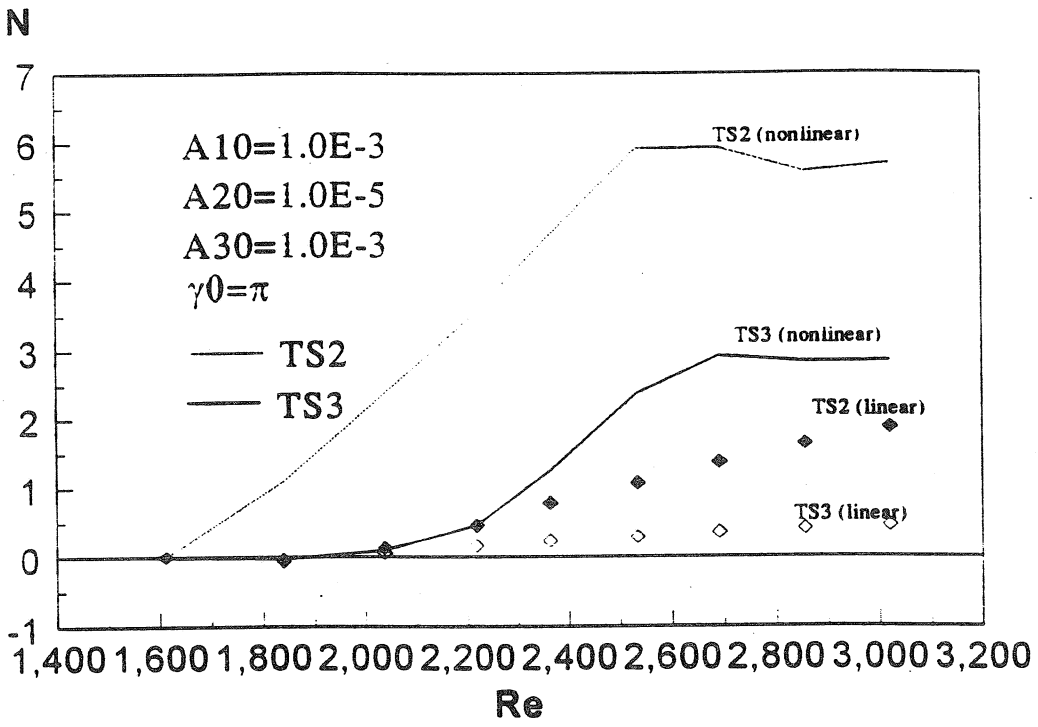


Figure 5: Compressible nonlinear TS N-factors for several initial amplitudes. Linear theory marked by symbols.

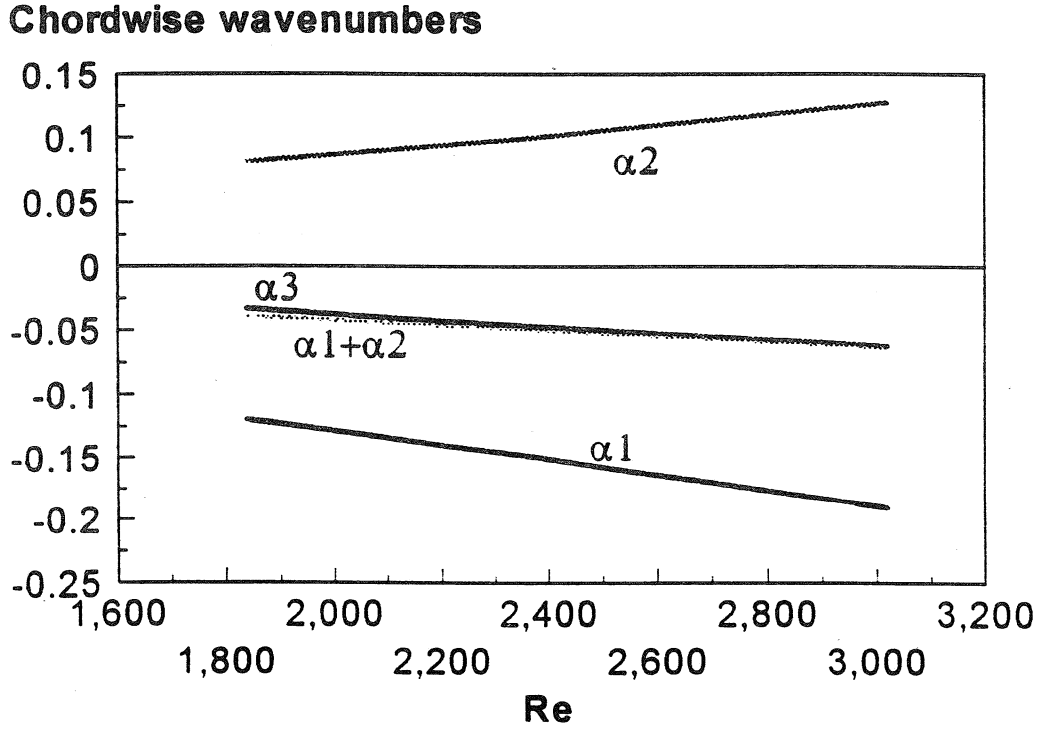


Figure 6: Compressible chordwise wavenumbers for a TS-TS-CF triad and the sum of the first two.

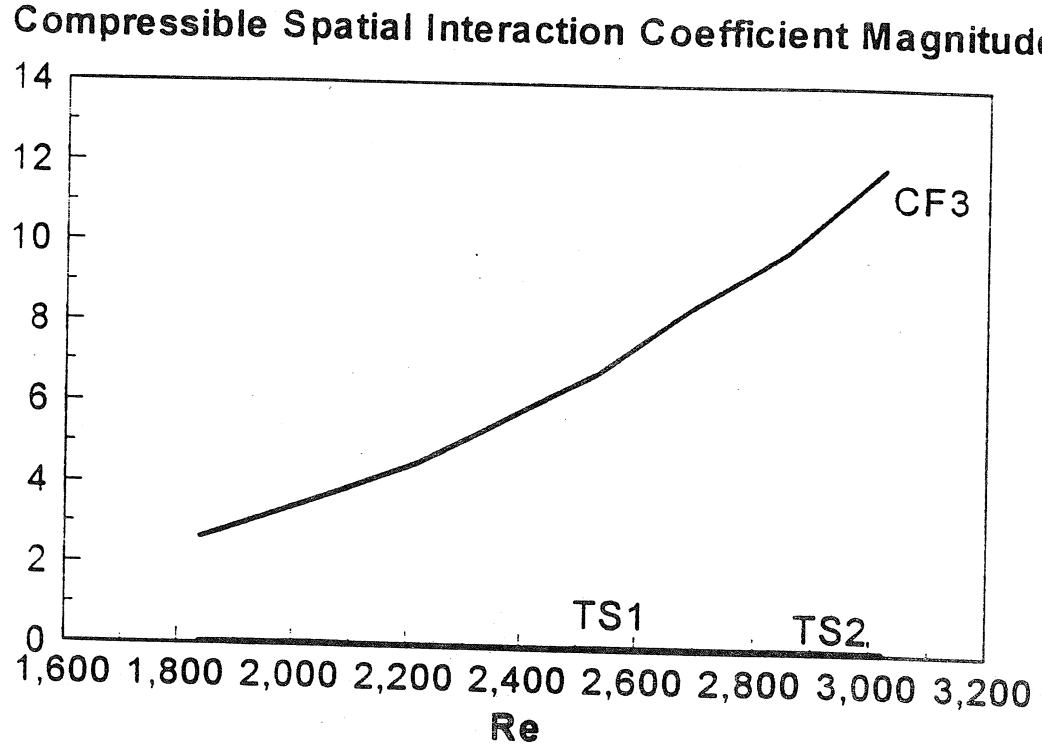


Figure 7: Compressible spatial interaction coefficients for a TS-TS-CF triad.

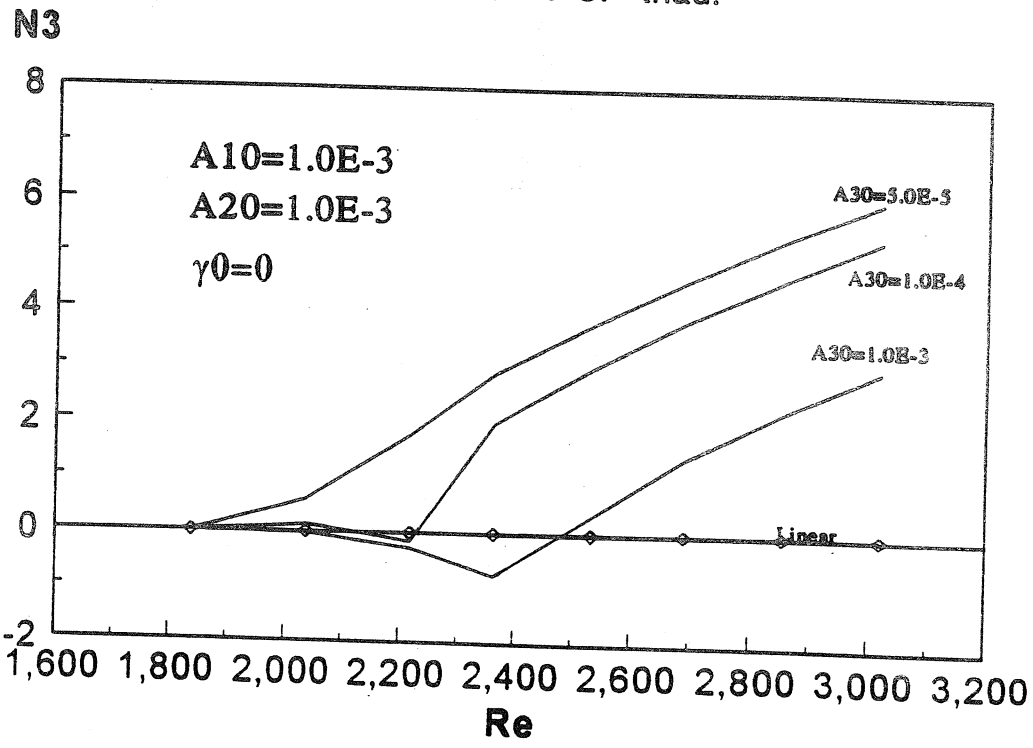


Figure 8: Compressible nonlinear N3-factor for a TS-TS-CF triad at several initial amplitudes. Symbols mark linear theory.

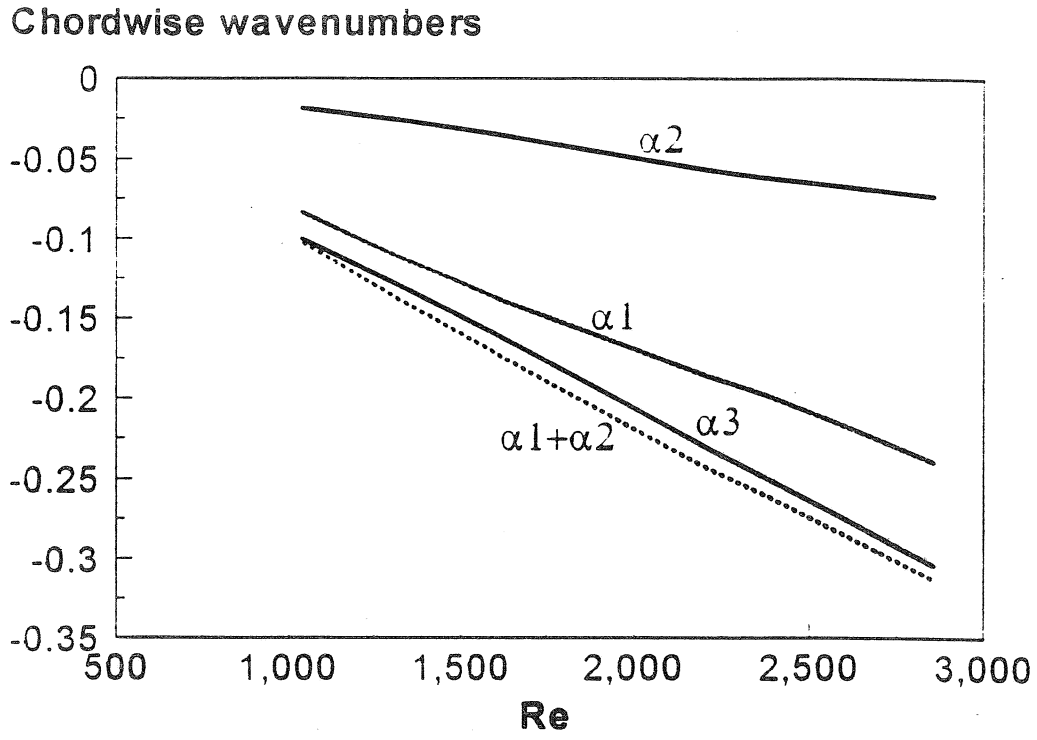


Figure 9: Compressible chordwise wavenumbers for a TS-CF-CF triad and the sum of the first two.

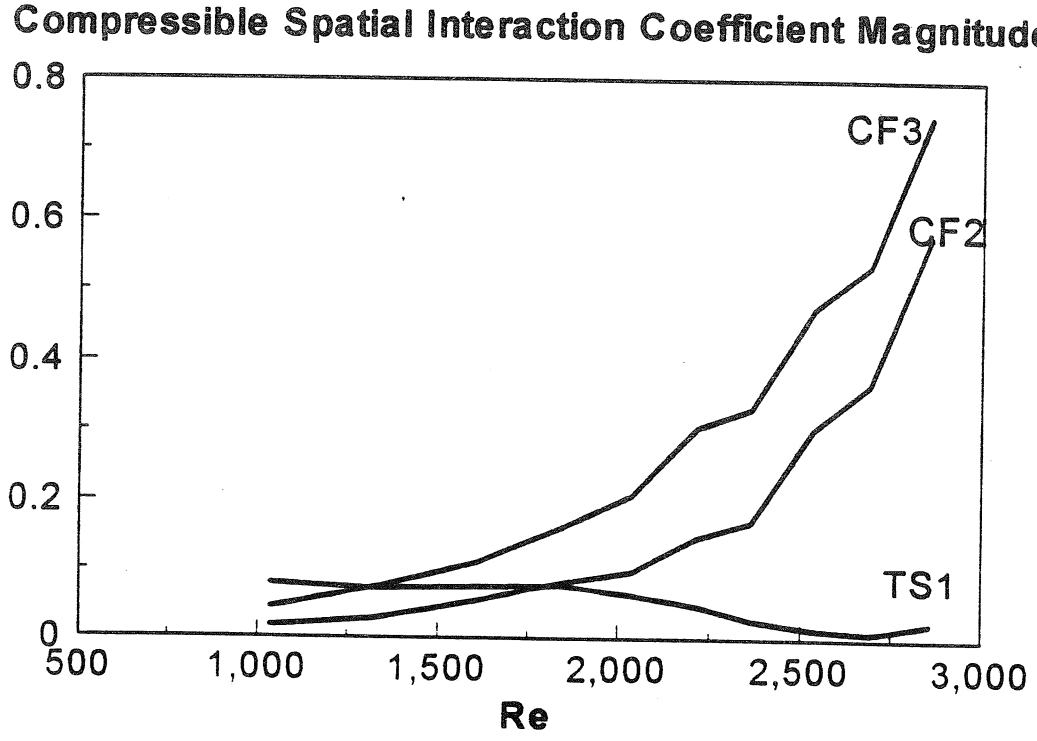


Figure 10: Compressible spatial interaction coefficients for a TS-CF-CF triad.

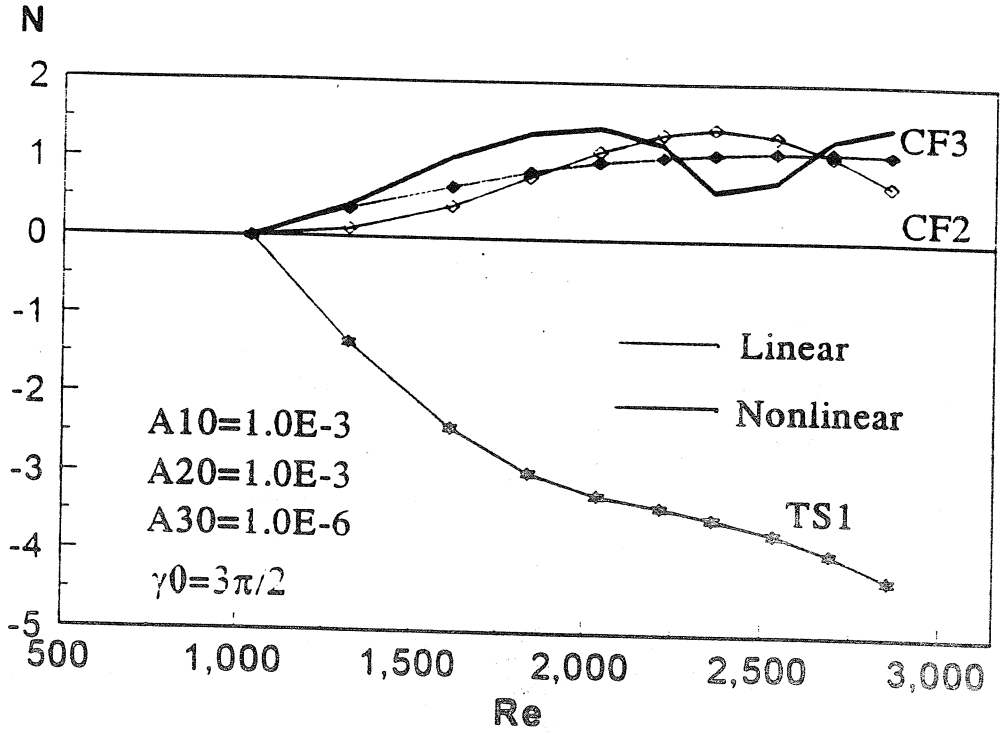


Figure 11: Compressible nonlinear N2-factor for a TS-CF-CF triad at several initial amplitudes. Symbols mark linear theory.

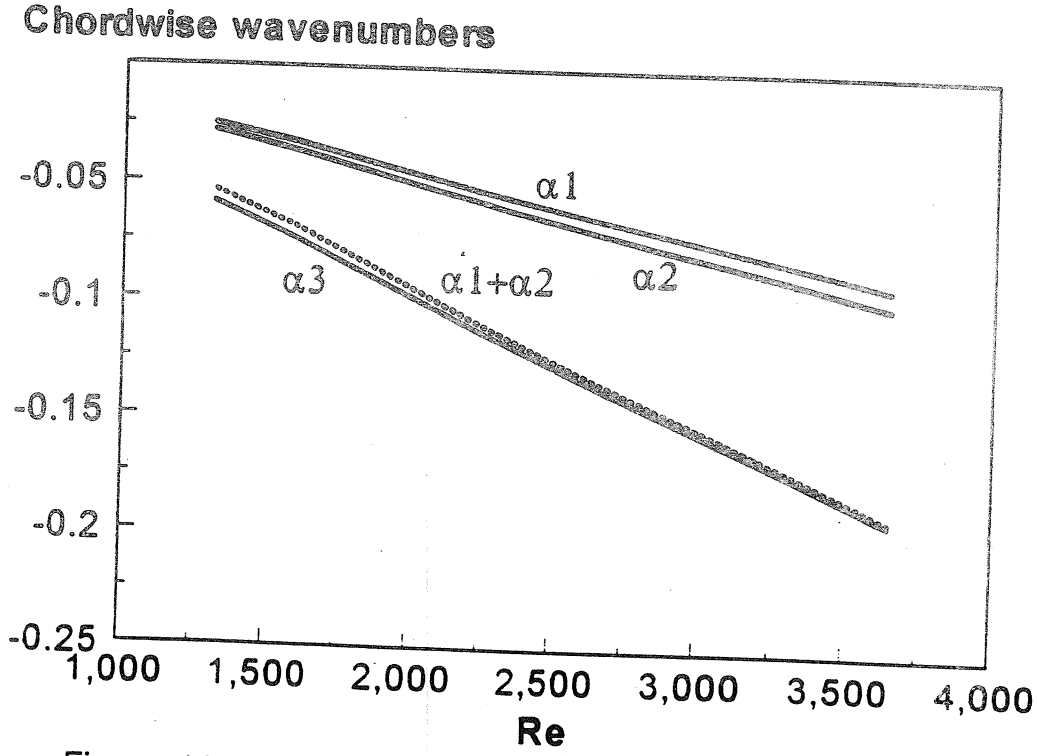


Figure 12: Compressible chordwise wavenumbers for a CF-CF-CF triad and the sum of the first two.

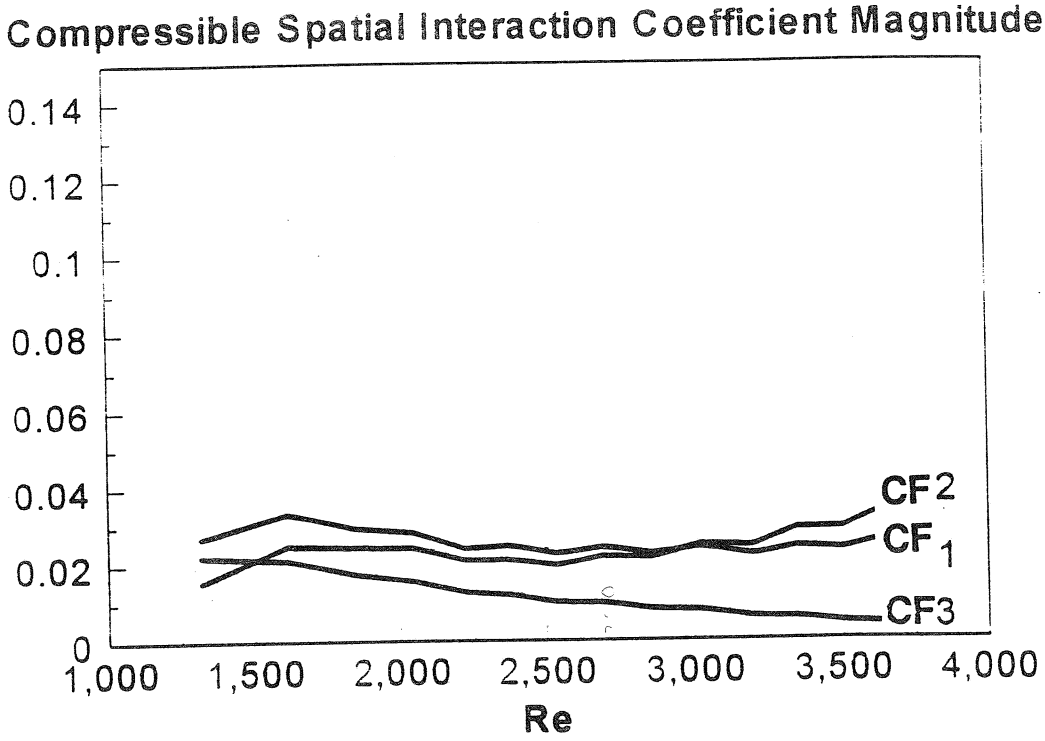


Figure 13: Compressible spatial interaction coefficients for a CF-CF-CF triad.

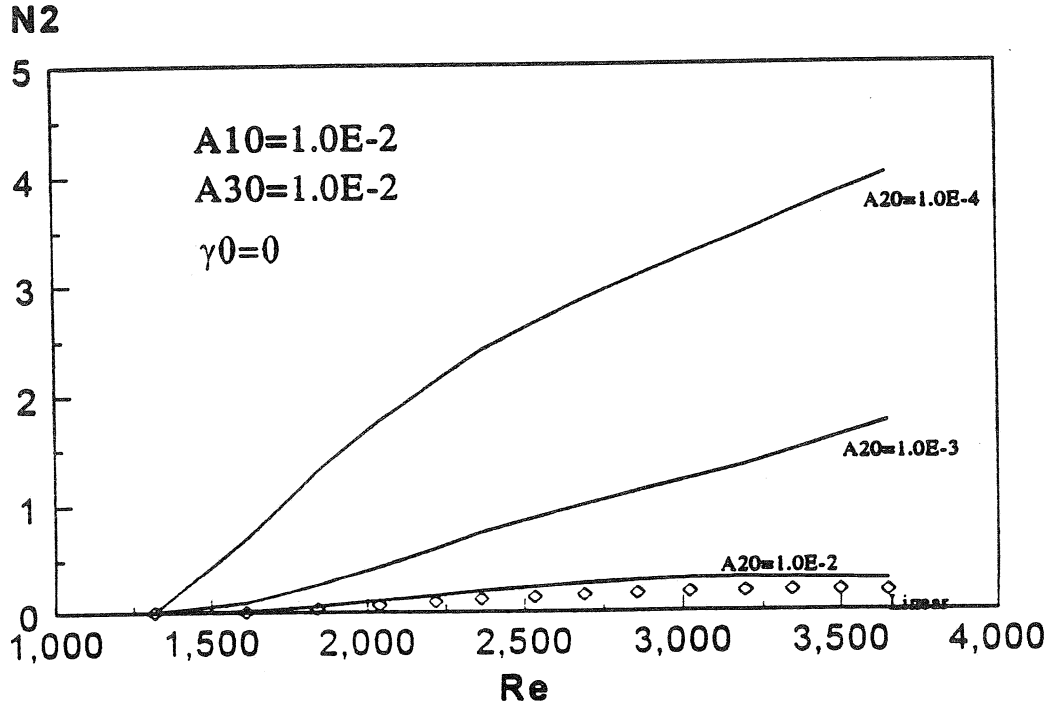


Figure 14: Compressible nonlinear N2-factor for a CF-CF-CF triad at several initial amplitudes. Linear theory marked by symbols.

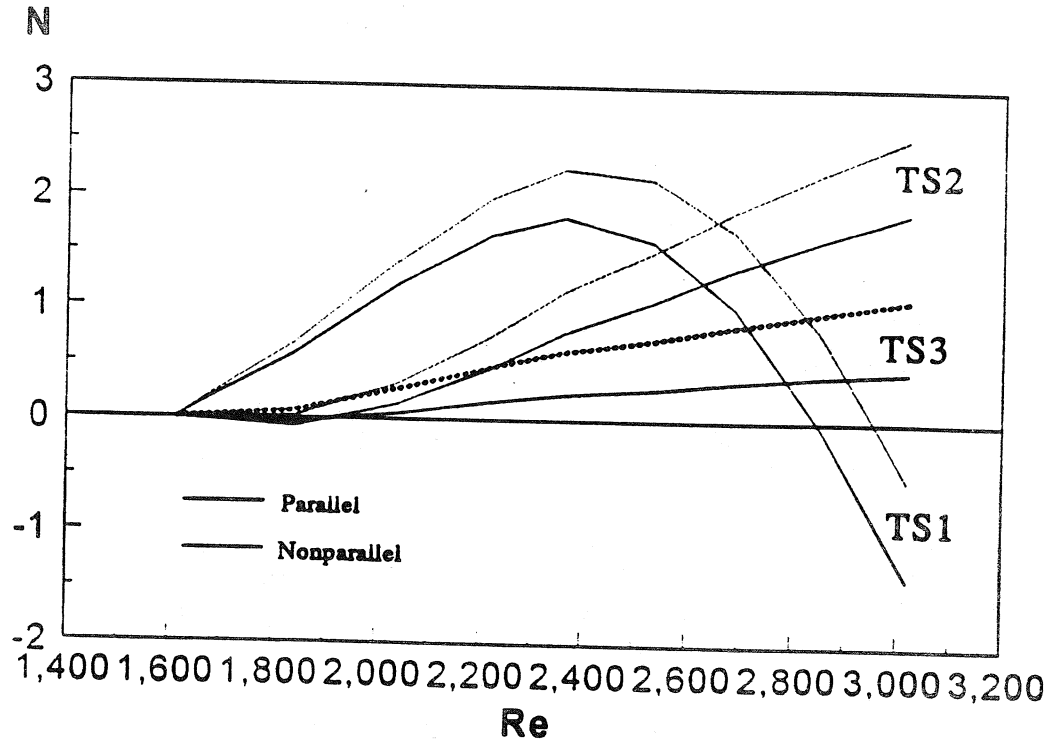


Figure 15: Compressible Linear N-factors for a TS-TS-TS triad. Parallel and nonparallel cases are shown.

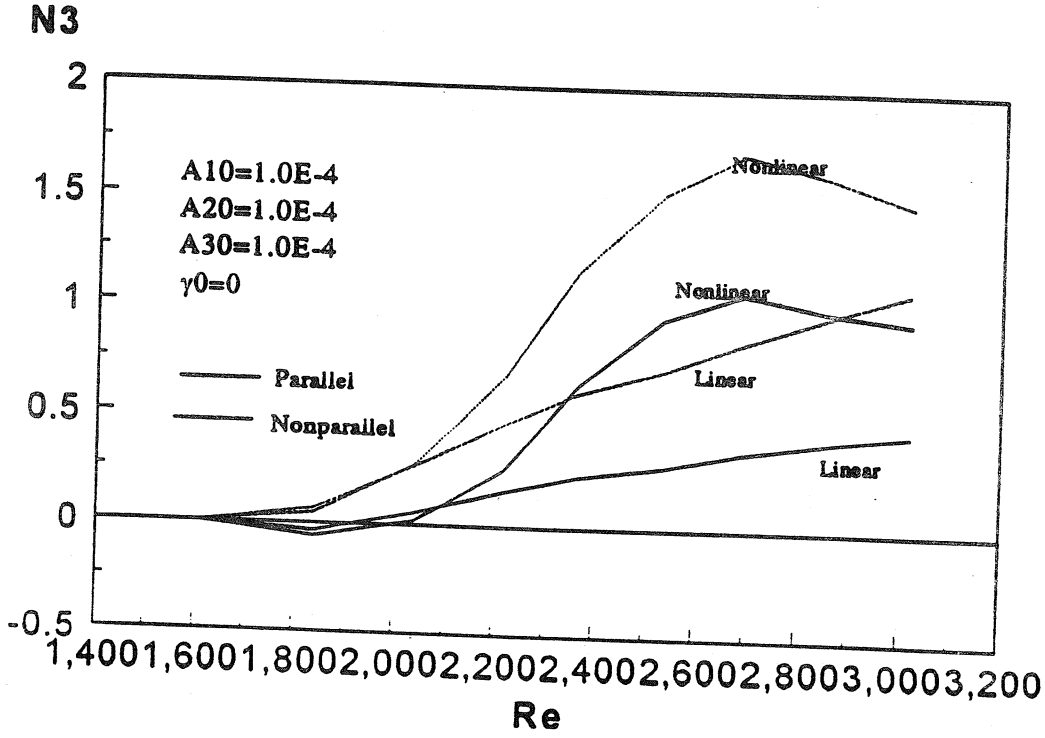


Figure 16: Compressible N-factors for parallel and nonparallel theories including nonlinear effects for a TS-TS-TS triad.

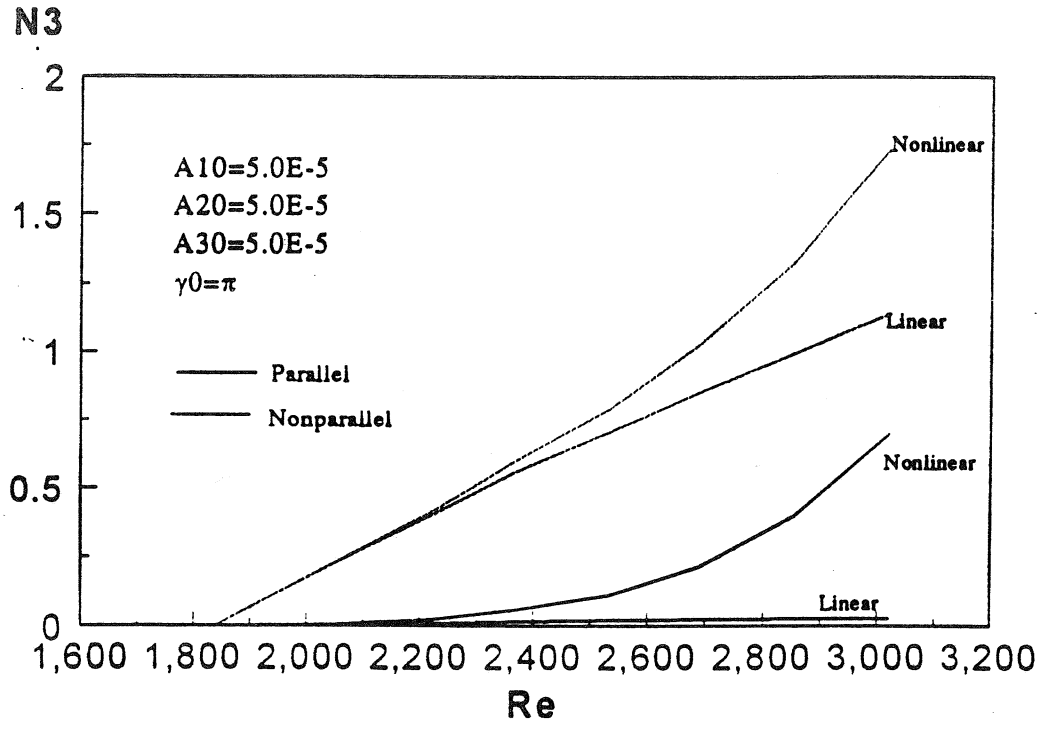


Figure 17: Compressible N-3 factor for parallel and nonparallel theories including nonlinear effects for a TS-TS-CF triad.

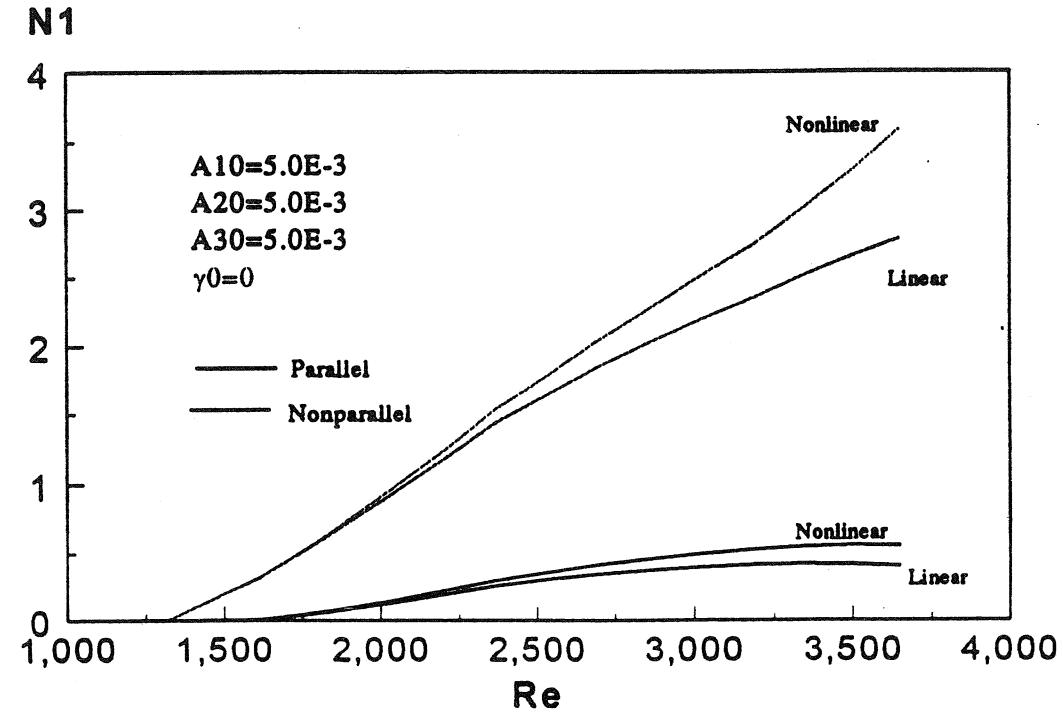


Figure 18: Compressible N1-factor for parallel and nonparallel theories including nonlinear effects for a CF-CF-CF triad.

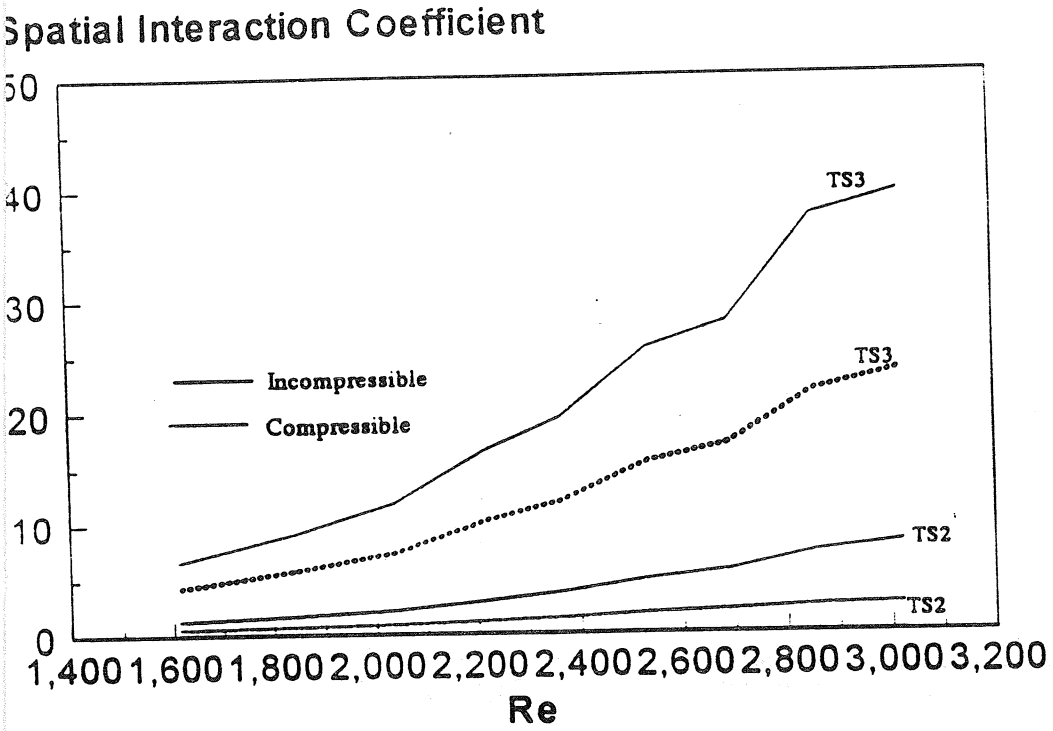


Figure 19: Compressible and incompressible spatial interaction coefficients for a Ts-TS-Ts triad.

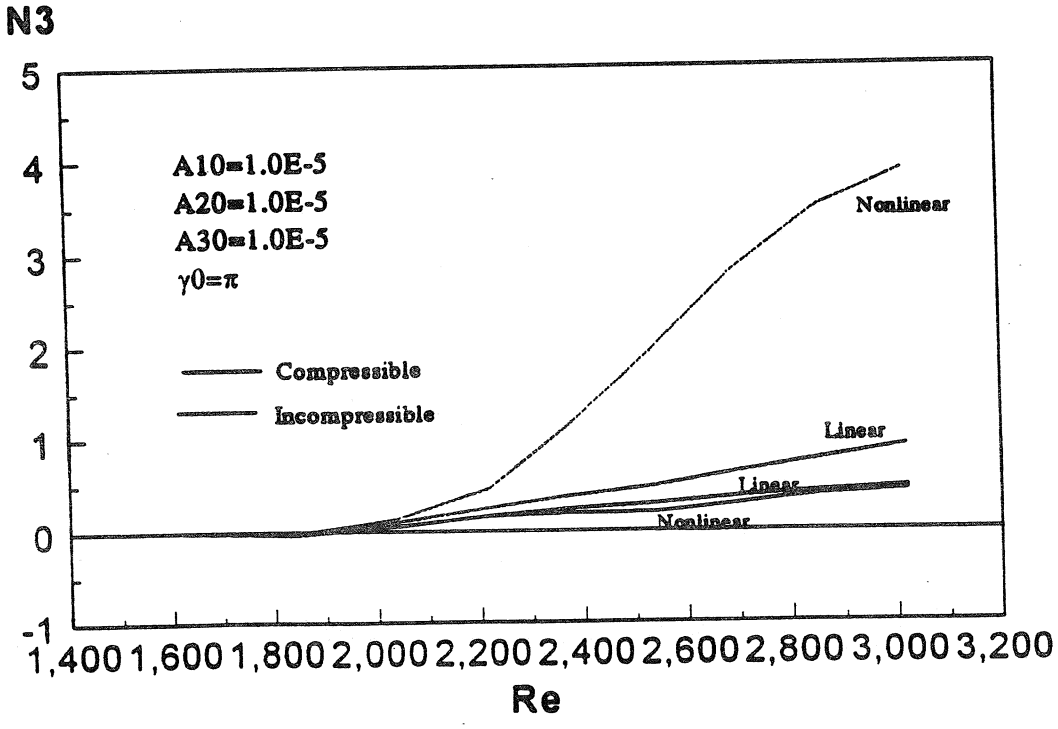


Figure 20: Compressible and incompressible N3-factors for a TS-TS-TS triad.

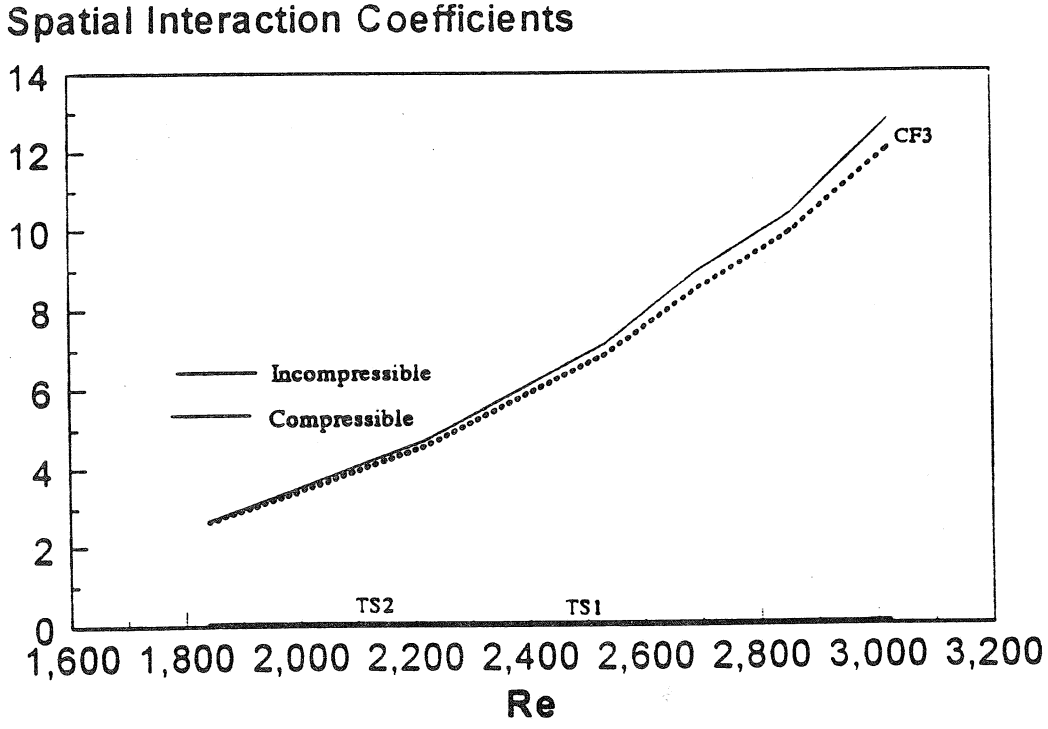


Figure 21: Compressible and incompressible spatial interaction coefficients for a TS-TS-CF triad.

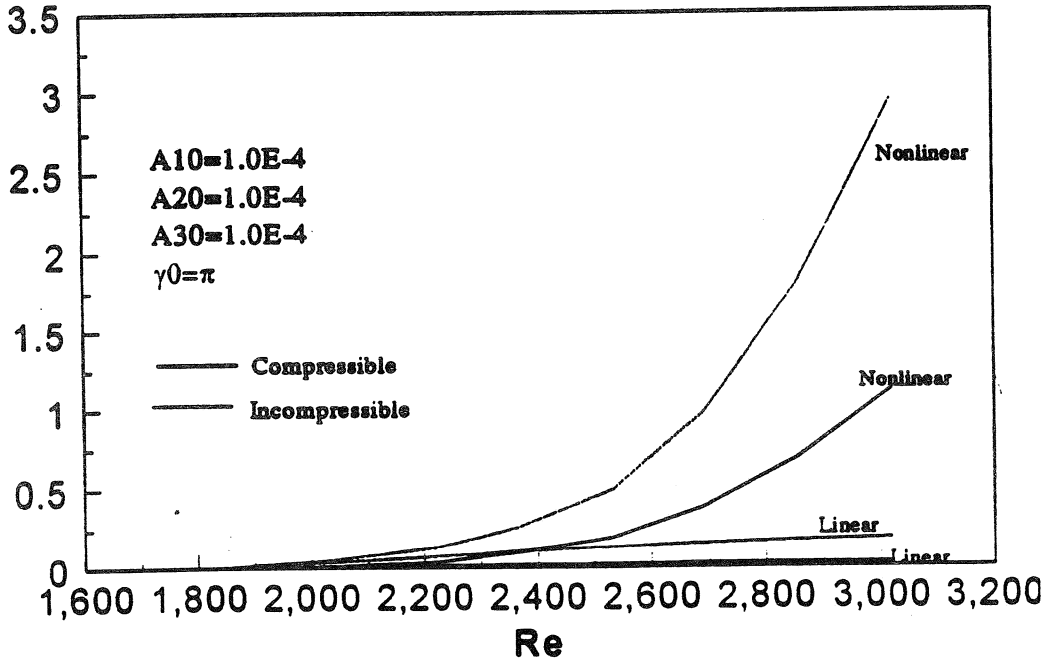


Figure 22: Compressible and incompressible N3-factors for a TS-TS-CF triad.

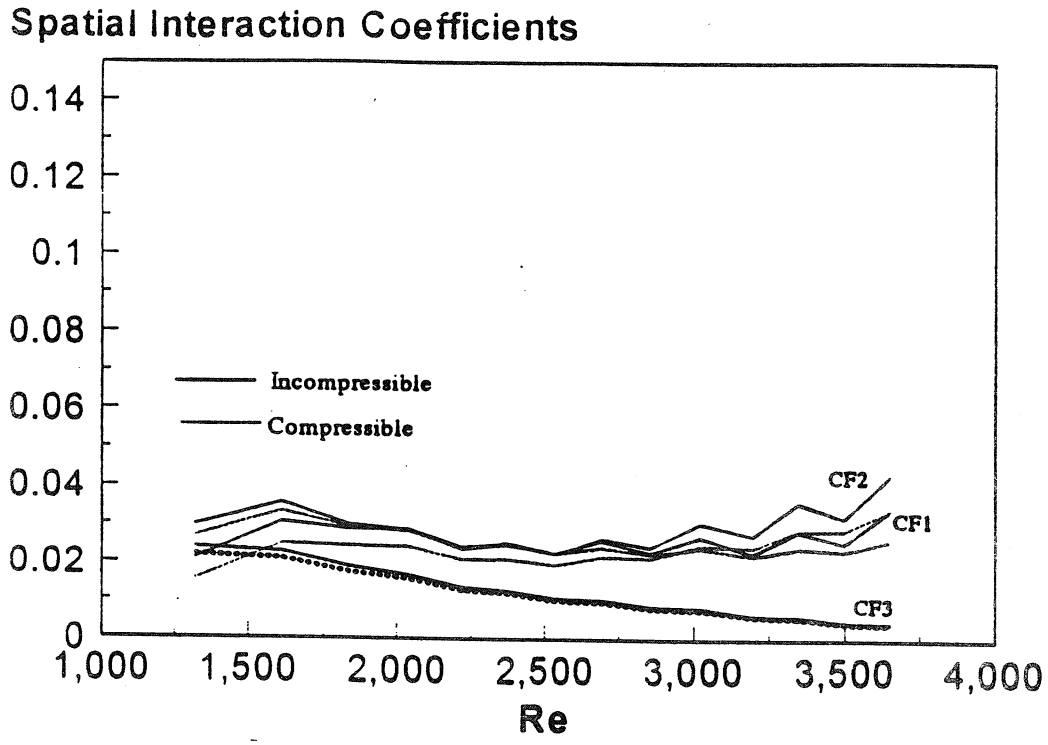


Figure 23: Compressible and incompressible spatial interaction coefficients for a CF-CF-CF triad.

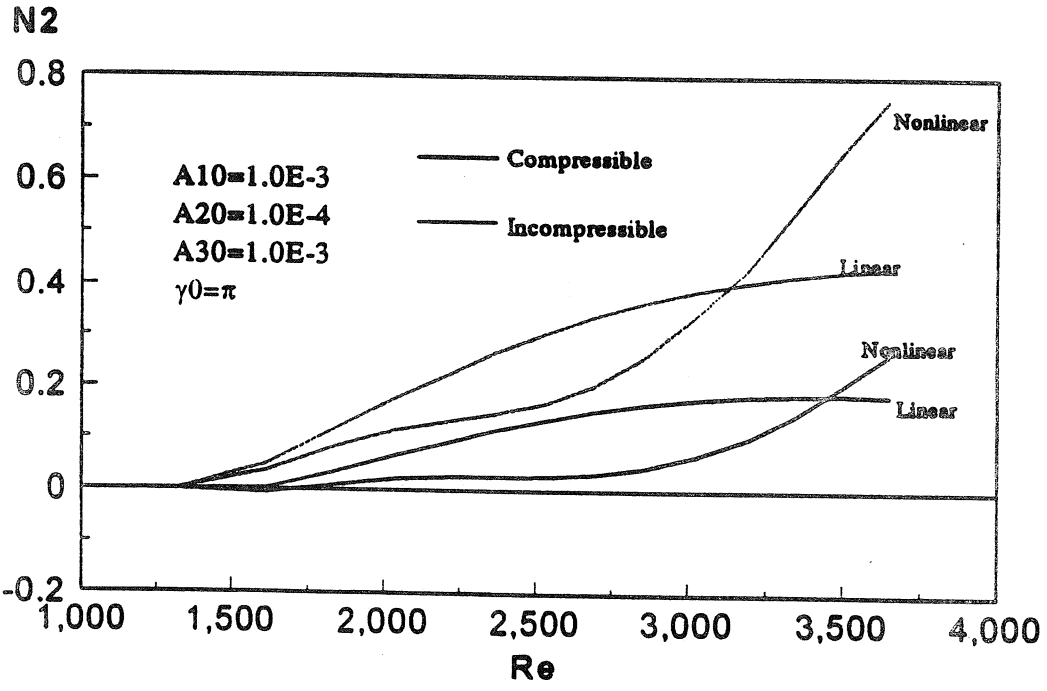


Figure 24: Compressible and incompressible N2-factors for a CF-CF-CF triad.

## List of Recent TAM Reports

| No. | Authors | Title | Date |
|---|---|---|---|
| 738 | Turner, J. A., and R. L. Weaver | Radiative transfer and multiple scattering of diffuse ultrasound in polycrystalline media—*Journal of the Acoustical Society of America* **96**, 3675–3681 (1994) | Nov. 1993 |
| 739 | Qi, Q., and R. E. Johnson | Resin flows through a porous fiber collection in pultrusion processing | Dec. 1993 |
| 740 | Weaver, R. L., W. Sachse, and K. Y. Kim | Transient elastic waves in a transversely isotropic plate—*Journal of Applied Mechanics*, in press (1996) | Dec. 1993 |
| 741 | Zhang, Y., and R. L. Weaver | Scattering from a thin random fluid layer—*Journal of the Acoustical Society of America* **96**, 1899–1909 (1994) | Dec. 1993 |
| 742 | Weaver, R. L., and W. Sachse | Diffusion of ultrasound in a glass bead slurry—*Journal of the Acoustical Society of America* **97**, 2094–2102 (1995) | Dec. 1993 |
| 743 | Sundermeyer, J. N., and R. L. Weaver | On crack identification and characterization in a beam by nonlinear vibration analysis—*Journal of Sound and Vibration* **183**, 857–872 (1995) | Dec. 1993 |
| 744 | Li, L., and N. R. Sottos | Predictions of static displacements in 1–3 piezocomposites—*Journal of Intelligent Materials Systems and Structures* **6**, 169–180 (1995) | Dec. 1993 |
| 745 | Jones, S. W. | Chaotic advection and dispersion—*Physica D* **76**, 55–69 (1994) | Jan. 1994 |
| 746 | Stewart, D. S., and J. Yao | Critical detonation shock curvature and failure dynamics: Developments in the theory of detonation shock dynamics—*Developments in Theoretical and Applied Mechanics* **17** (1994) | Feb. 1994 |
| 747 | Mei, R., and R. J. Adrian | Effect of Reynolds-number-dependent turbulence structure on the dispersion of fluid and particles—*Journal of Fluids Engineering* **117**, 402-409 (1995) | Feb. 1994 |
| 748 | Liu, Z.-C., R. J. Adrian, and T. J. Hanratty | Reynolds-number similarity of orthogonal decomposition of the outer layer of turbulent wall flow—*Physics of Fluids* **6**, 2815–2819 (1994) | Feb. 1994 |
| 749 | Barnhart, D. H., R. J. Adrian, and G. C. Papen | Phase-conjugate holographic system for high-resolution particle image velocimetry—*Applied Optics* **33**, 7159–7170 (1994) | Feb. 1994 |
| 750 | Qi, Q., W. D. O'Brien Jr., and J. G. Harris | The propagation of ultrasonic waves through a bubbly liquid into tissue: A linear analysis—*IEEE Transactions on Ultrasonics, Ferroelectrics and Frequency Control* **42**, 28–36 (1995) | Mar. 1994 |
| 751 | Mittal, R., and S. Balachandar | Direct numerical simulation of flow past elliptic cylinders—*Journal of Computational Mechanics*, in press (1996) | May 1994 |
| 752 | Students in TAM 293–294 | Thirty-first student symposium on engineering mechanics, J. W. Phillips, coordinator: Selected senior projects by D. N. Anderson, J. R. Dahlen, M. J. Danyluk, A. M. Dreyer, K. M. Durkin, J. J. Kriegsmann, J. T. McGonigle, and V. Tyagi | May 1994 |
| 753 | Thoroddsen, S. T. | The failure of the Kolmogorov refined similarity hypothesis in fluid turbulence—*Physics of Fluids* **7**, 691–693 (1995) | May 1994 |
| 754 | Turner, J. A., and R. L. Weaver | Time dependence of multiply scattered diffuse ultrasound in polycrystalline media—*Journal of the Acoustical Society of America* **97**, 2639–2644 (1995) | June 1994 |
| 755 | Riahi, D. N. | Finite-amplitude thermal convection with spatially modulated boundary temperatures—*Proceedings of the Royal Society of London A* **449**, 459–478 (1995) | June 1994 |
| 756 | Riahi, D. N. | Renormalization group analysis for stratified turbulence—*International Journal of Mathematics and Mathematical Sciences*, in press (1996) | June 1994 |
| 757 | Riahi, D. N. | Wave-packet convection in a porous layer with boundary imperfections—*Journal of Fluid Mechanics*, in press (1996) | June 1994 |

| No. | Authors | Title | Date |
|---|---|---|---|
| 758 | Jog, C. S., and R. B. Haber | Stability of finite element models for distributed-parameter optimization and topology design—*Computer Methods in Applied Mechanics and Engineering,* in press (1996). | July 1994 |
| 759 | Qi, Q., and G. J. Brereton | Mechanisms of removal of micron-sized particles by high-frequency ultrasonic waves—*IEEE Transactions on Ultrasonics, Ferroelectrics and Frequency Control* **42**, 619–629 (1995) | July 1994 |
| 760 | Shawki, T. G. | On shear flow localization with traction-controlled boundaries—*International Journal of Solids and Structures* **32**, 2751–2778 (1995) | July 1994 |
| 761 | Balachandar, S., D. A. Yuen, and D. M. Reuteler | High Rayleigh number convection at infinite Prandtl number with temperature-dependent viscosity | July 1994 |
| 762 | Phillips, J. W. | Arthur Newell Talbot—Proceedings of a conference to honor TAM's first department head and his family | Aug. 1994 |
| 763 | Man., C. S., and D. E. Carlson | On the traction problem of dead loading in linear elasticity with initial stress—*Archive for Rational Mechanics and Analysis* **128**, 223–247 (1994) | Aug. 1994 |
| 764 | Zhang, Y., and R. L. Weaver | Leaky Rayleigh wave scattering from elastic media with random microstructures | Aug. 1994 |
| 765 | Cortese, T. A., and S. Balachandar | High-performance spectral simulation of turbulent flows in massively parallel machines with distributed memory—*International Journal of Supercomputer Applications* **9**, 185–202 (1995) | Aug. 1994 |
| 766 | Balachandar, S. | Signature of the transition zone in the tomographic results extracted through the eigenfunctions of the two-point correlation—*Geophysical Research Letters* **22**, 1941–1944 (1995) | Sept. 1994 |
| 767 | Piomelli, U. | Large-eddy simulation of turbulent flows | Sept. 1994 |
| 768 | Harris, J. G., D. A. Rebinsky, and G. R. Wickham | An integrated model of scattering from an imperfect interface—*Journal of the Acoustical Society of America,* in press (1996) | Sept. 1994 |
| 769 | Hsia, K. J., and Z.-Q. Xu | The mathematical framework and an approximate solution of surface crack propagation under hydraulic pressure loading—*International Journal of Fracture,* in press (1996) | Sept. 1994 |
| 770 | Balachandar, S. | Two-point correlation and its eigen-decomposition for optimal characterization of mantle convection | Oct. 1994 |
| 771 | Lufrano, J. M., and P. Sofronis | Numerical analysis of the interaction of solute hydrogen atoms with the stress field of a crack—*International Journal of Solids and Structures,* in press (1996) | Oct. 1994 |
| 772 | Aref, H., and S. W. Jones | Motion of a solid body through ideal fluid | Oct. 1994 |
| 773 | Stewart, D. S., T. D. Aslam, J. Yao, and J. B. Bdzil | Level-set techniques applied to unsteady detonation propagation—In "Modeling in Combustion Science," *Lecture Notes in Physics* (1995) | Oct. 1994 |
| 774 | Mittal, R., and S. Balachandar | Effect of three-dimensionality on the lift and drag of circular and elliptic cylinders—*Physics of Fluids* **7**, 1841–1865 (1995) | Oct. 1994 |
| 775 | Stewart, D. S., T. D. Aslam, and J. Yao | On the evolution of cellular detonation | Nov. 1994 *Revised* Jan. 1996 |
| 776 | Aref, H. | On the equilibrium and stability of a row of point vortices—*Journal of Fluid Mechanics* **290**, 167–181 (1995) | Nov. 1994 |
| 777 | Cherukuri, H. P., T. G. Shawki, and M. El-Raheb | An accurate finite-difference scheme for elastic wave propagation in a circular disk—*Journal of the Acoustical Society of America,* in press (1996) | Nov. 1994 |

## List of Recent TAM Reports (cont'd)

| No. | Authors | Title | Date |
|---|---|---|---|
| 778 | Li, L., and N. R. Sottos | Improving hydrostatic performance of 1–3 piezocomposites—*Journal of Applied Physics* **77**, 4595–4603 (1995) | Dec. 1994 |
| 779 | Phillips, J. W., D. L. de Camara, M. D. Lockwood, and W. C. C. Grebner | Strength of silicone breast implants—*Plastic and Reconstructive Surgery* **97**, in press (1996) | Jan. 1995 |
| 780 | Xin, Y.-B., K. J. Hsia, and D. A. Lange | Quantitative characterization of the fracture surface of silicon single crystals by confocal microscopy—*Journal of the American Ceramics Society* **78**, 3201-3208 (1995) | Jan. 1995 |
| 781 | Yao, J., and D. S. Stewart | On the dynamics of multi-dimensional detonation—*Journal of Fluid Mechanics* **309**, 225-275 (1996) | Jan. 1995 |
| 782 | Riahi, D. N., and T. L. Sayre | Effect of rotation on the structure of a convecting mushy layer—*Acta Mechanica,* in press (1996) | Feb. 1995 |
| 783 | Batchelor, G. K., and TAM faculty and students | A conversation with Professor George K. Batchelor | Feb. 1995 |
| 784 | Sayre, T. L., and D. N. Riahi | Effect of rotation on flow instabilities during solidification of a binary alloy | Feb. 1995 |
| 785 | Xin, Y.-B., and K. J. Hsia | A technique to generate straight surface cracks for studying the dislocation nucleation condition in brittle materials —*Acta Metallurgica et Materialia* **44**, 845-853 (1996). | Mar. 1995 |
| 786 | Riahi, D. N. | Finite bandwidth, long wavelength convection with boundary imperfections: Near-resonant wavelength excitation | Mar. 1995 |
| 787 | Turner, J. A., and R. L. Weaver | Average response of an infinite plate on a random foundation—*Journal of the Acoustical Society of America* **99**, in press (1996) | Mar. 1995 |
| 788 | Weaver, R. L., and D. Sornette | The range of spectral correlations in pseudointegrable systems: GOE statistics in a rectangular membrane with a point scatterer—*Physical Review E* **52**, 341 (1995) | April 1995 |
| 789 | Students in TAM 293–294 | Thirty-second student symposium on engineering mechanics, J. W. Phillips, coordinator: Selected senior projects by K. F. Anderson, M. B. Bishop, B. C. Case, S. R. McFarlin, J. M. Nowakowski, D. W. Peterson, C. V. Robertson, and C. E. Tsoukatos | April 1995 |
| 790 | Figa, J., and C. J. Lawrence | Linear stability analysis of a gravity-driven Newtonian coating flow on a planar incline | May 1995 |
| 791 | Figa, J., and C. J. Lawrence | Linear stability analysis of a gravity-driven viscosity-stratified Newtonian coating flow on a planar incline | May 1995 |
| 792 | Cherukuri, H. P., and T. G. Shawki | On shear band nucleation and the finite propagation speed of thermal disturbances—*International Journal of Solids and Structures,* in press (1996) | May 1995 |
| 793 | Harris, J. G. | Modeling scanned acoustic imaging of defects at solid interfaces—Chapter in *IMA Workshop on Inverse Problems in Wave Propagation,* Springer-Verlag, in press (1996) | May 1995 |
| 794 | Sottos, N. R., J. M. Ockers, and M. J. Swindeman | Thermoelastic properties of plain weave composites for multilayer circuit board applications | May 1995 |
| 795 | Aref, H., and M. A. Stremler | On the motion of three point vortices in a periodic strip—*Journal of Fluid Mechanics,* in press (1996). | June 1995 |
| 796 | Barenblatt, G. I., and N. Goldenfeld | Does fully-developed turbulence exist? Reynolds number independence versus asymptotic covariance—*Physics of Fluids* **7**, 3078–3082 (1995) | June 1995 |

| No. | Authors | Title | Date |
|---|---|---|---|
| 797 | Aslam, T. D., J. B. Bdzil, and D. S. Stewart | Level set methods applied to modeling detonation shock dynamics—*Journal of Computational Physics,* in press (1996) | June 1995 |
| 798 | Nimmagadda, P. B. R., and P. Sofronis | The effect of interface slip and diffusion on the creep strength of fiber and particulate composite materials—*Mechanics of Materials,* in press (1996) | July 1995 |
| 799 | Hsia, K. J., T.-L. Zhang, and D. F. Socie | Effect of crack surface morphology on the fracture behavior under mixed mode loading —*ASTM Special Technical Publication* 1296, in press (1996) | July 1995 |
| 800 | Adrian, R. J. | Stochastic estimation of the structure of turbulent fields | Aug. 1995 |
| 801 | Riahi, D. N. | Perturbation analysis and modeling for stratified turbulence | Aug. 1995 |
| 802 | Thoroddsen, S. T. | Conditional sampling of dissipation in high Reynolds number turbulence —*Physics of Fluids,* in press (1996) | Aug. 1995 |
| 803 | Riahi, D. N. | On the structure of an unsteady convecting mushy layer | Aug. 1995 |
| 804 | Meleshko, V. V. | Equilibrium of an elastic rectangle: The Mathieu–Inglis–Pickett solution revisited—*Journal of Elasticity* **40**, 207-238 (1995) | Aug. 1995 |
| 805 | Jonnalagadda, K., G. E. Kline, and N. R. Sottos | Local displacements and load transfer in shape memory alloy composites | Aug. 1995 |
| 806 | Nimmagadda, P. B. R., and P. Sofronis | On the calculation of the matrix–reinforcement interface diffusion coefficient in composite materials at high temperatures—*Acta Metallurgica et Materialia*, in press (1996) | Aug. 1995 |
| 807 | Carlson, D. E., and D. A. Tortorelli | On hyperelasticity with internal constraints—*Journal of Elasticity*, in press (1996) | Aug. 1995 |
| 808 | Sayre, T. L., and D. N. Riahi | Oscillatory instabilities of the liquid and mushy layers during solidification of alloys under rotational constraint—*Acta Mechanica,* in press (1996) | Sept. 1995 |
| 809 | Xin, Y.-B., and K. J. Hsia | Simulation of the brittle-ductile transition in silicon single crystals using dislocation mechanics | Oct. 1995 |
| 810 | Ulysse, P., and R. E. Johnson | A plane-strain upper-bound analysis of unsymmetrical single-hole and multi-hole extrusion processes | Oct. 1995 |
| 811 | Fried, E. | Continua described by a microstructural field—*Zeitschrift für angewandte Mathematik und Physik,* in press (1996) | Nov. 1995 |
| 812 | Mittal, R., and S. Balachandar | Autogeneration of three-dimensional vortical structures in the near wake of a circular cylinder | Nov. 1995 |
| 813 | Segev, R., E. Fried, and G. de Botton | Force theory for multiphase bodies—*Journal of Geometry and Physics*, in press (1996) | Dec. 1995 |
| 814 | Weaver, R. L. | The effect of an undamped finite-degree-of-freedom "fuzzy" substructure: Numerical solutions and theoretical discussion | Jan. 1996 |
| 815 | Haber, R. B., C. S. Jog, and M. P. Bensøe | A new approach to variable-topology shape design using a constraint on perimeter—*Structural Optimization* **11**, 1-12 (1996) | Feb. 1996 |
| 816 | Xu, Z.-Q., and K. J. Hsia | A numerical solution of a surface crack under cyclic hydraulic pressure loading | Mar. 1996 |
| 817 | Adrian, R. J. | Bibliography of particle velocimetry using imaging methods: 1917–1995—*Produced and distributed in cooperation with TSI, Inc., St. Paul, Minn.* | Mar. 1996 |
| 818 | Fried, E., and G. Grach | An order-parameter based theory as a regularization of a sharp-interface theory for solid–solid phase transitions—*Archive for Rational Mechanics and Analysis,* in press (1996) | Mar. 1996 |
| 819 | Vonderwell, M. P., and D. N. Riahi | Resonant instability mode triads in the compressible boundary-layer flow over a swept wing | Mar. 1996 |